Spring 1990

A New Determination of Pacific-Kula Relative Motions

Harold J. (Harold John) Cashman
Western Washington University, hjcashman@whatcomenvironmental.com

A NEW DETERMINATION OF PACIFIC-KULA RELATIVE MOTIONS

by

Harold J. Cashman

Accepted in Partial Completion
of the Requirements for the Degree
Master of Science

Dean of Graduate School

Advisory Committee

Chair

MASTER'S THESIS

In presenting this thesis in partial fulfillment of the requirements for a master's degree at Western Washington University, I grant to Western Washington University the non-exclusive royalty-free right to archive, reproduce, distribute, and display the thesis in any and all forms, including electronic format, via any digital library mechanisms maintained by WWU.

I represent and warrant this is my original work, and does not infringe or violate any rights of others. I warrant that I have obtained written permissions from the owner of any third party copyrighted material included in these files.

I acknowledge that I retain ownership rights to the copyright of this work, including but not limited to the right to use all or part of this work in future works, such as articles or books.

Library users are granted permission for individual, research and non-commercial reproduction of this work for educational purposes only. Any further digital posting of this document requires specific permission from the author.

Any copying or publication of this thesis for commercial purposes, or for financial gain, is not allowed without my written permission.

Harold Cashman
February 28, 2018

A NEW DETERMINATION OF PACIFIC-KULA RELATIVE MOTIONS

A Thesis Presented to the Faculty of
Western Washington University

In Partial Fulfillment
of the Requirements for the Degree
Master of Science

by

Harold J. Cashman

June, 1990

ABSTRACT

A new method is presented and used to determine estimates of instantaneous relative motion vectors for the Pacific plate relative to the Farallon and Kula plates between magnetic chrons 34 and 24 (84 to 56 Ma). A weighted chi-square minimization technique was employed that has as input sequential magnetic anomaly picks taken from original ship-track profiles, and fracture-zone azimuths estimated from bathymetric control and offsets in magnetic lineations. Assignment of errors to the input data allows the use of critical chi-square limits to obtain confidence intervals on pole locations and their angular rates. Eleven distinctive magnetic anomalies chosen as control points within the 28 million year time span result in ten possible instantaneous relative motion poles. Within the uncertainties, 3 distinct pole positions have been modeled for Pacific-Kula spreading spanning the time between chrons 34 to 33 (84 to 77 Ma), 33 to 25 (77 to 59 Ma), and 25 to 24 (59 to 56 Ma). Six significant rate changes are seen within the interval between chrons 33 and 25. These results are consistent with but more detailed than earlier hypotheses, which suggested that Pacific-Kula relative motions can be described by a single pole location between chron 32 and 25, accompanied by three changes in angular rates. Previous workers have determined that Pacific-Farallon relative motion can be described by two pole locations; this study used these pole positions to update Pacific-Farallon angular rates for the ten time intervals.

Updated relative motions were used in combination with the trace of the Pacific-Farallon-Kula (PFK) triple junction to investigate the possibility of asymmetric spreading. Except for two time intervals, the updated relative motions agree well with the observed migration of the PFK triple junction (as seen at the apexes of the Great Magnetic Bight) which implies, at least on average, consistency with the assumption of symmetric spreading.

Results of this study differ from those of previous studies in the greater number of relative motion changes found, presumably in response to changes along Kula and Farallon subduction zones. These updated models should provide increased insight into the cause of changing tectonic environments along western North America during the late Cretaceous and early Tertiary.

Acknowledgements

First and foremost I would like to thank Dave and Debbi Engebretson for their constant support throughout my graduate career. I feel extremely lucky to have Dave as my committee chairman who is a mentor, friend, and party animal! You guys are the best! Special thanks also to Russ Burmester, for his valuable assistance with this thesis and for his willingness to share his climbing skills. Thanks also to Jim Talbot, the third member of my committee, for his speedy review of this manuscript.

I would like to thank all of the Geology Department faculty for their support. The classes I have taken here at Western will benefit me greatly in the future. Patty Combs and Vicki Critchlow deserve special thanks for all their guidance and patience. I would also like to thank George Mustoe for providing such a wonderful working environment here in the Geology Department and the entire E. S. building.

Special thanks go out to Kevin Kelley, my housemate and friend, for being such a solid bro. I also want to thank my parents and siblings, whose love and support have helped me complete this thesis. Thank you, Jeanne, for everything!

This research was supported by a Geology Department Graduate Research Assistantship and by National Science Foundation grant OCE 8816952.

TABLE OF CONTENTS

LIST OF FIGURES

LIST OF TABLES

Introduction

The topic of this research is the history of plate interactions between the Pacific, Kula, and Farallon plates from 84 to 56 Ma as recorded by magnetic chrons and fracture zones of the Great Magnetic Bight (GMB) located in the north Pacific basin (Figure 1). Results of this work include an updated set of Pacific-Kula relative motion poles with their uncertainties and a revision of Pacific-Farallon spreading rates. A new method is described and used to delineate these motions and the results are used to test the assumption of symmetric seafloor spreading in the vicinity of the GMB. Although not treated here, a detailed history of Pacific-Kula relative motions will enhance the understanding of Kula-North America plate interactions in the late Cretaceous and early Tertiary, which are in part responsible for the present geometry of accreted terranes along the western margin of North America.

Crust between the Aleutian Trench and the Chinook Trough contains the magnetic record used to delineate Pacific-Kula motion (Figure 1). Late-Cretaceous through Eocene magnetic isochrons and fracture zones in the vicinity of the GMB, located between 175°E - 205°E and 43°N - 53°N in the northern Pacific basin, uniquely record the Pacific side of Pacific-Kula and Pacific-Farallon spreading. This data set describes the motion of the Kula and Farallon ridges relative to the Pacific plate, as well as the migration of the Pacific-Farallon-Kula (PFK) triple junction (Figure 1). Determination of the relative motions between the Pacific plate and the Pacific-Kula ridge involved the identification and tectonic analysis of east-west trending magnetic isochrons 34 (84.00 Ma) through 24 (55.64 Ma). North-south lineations

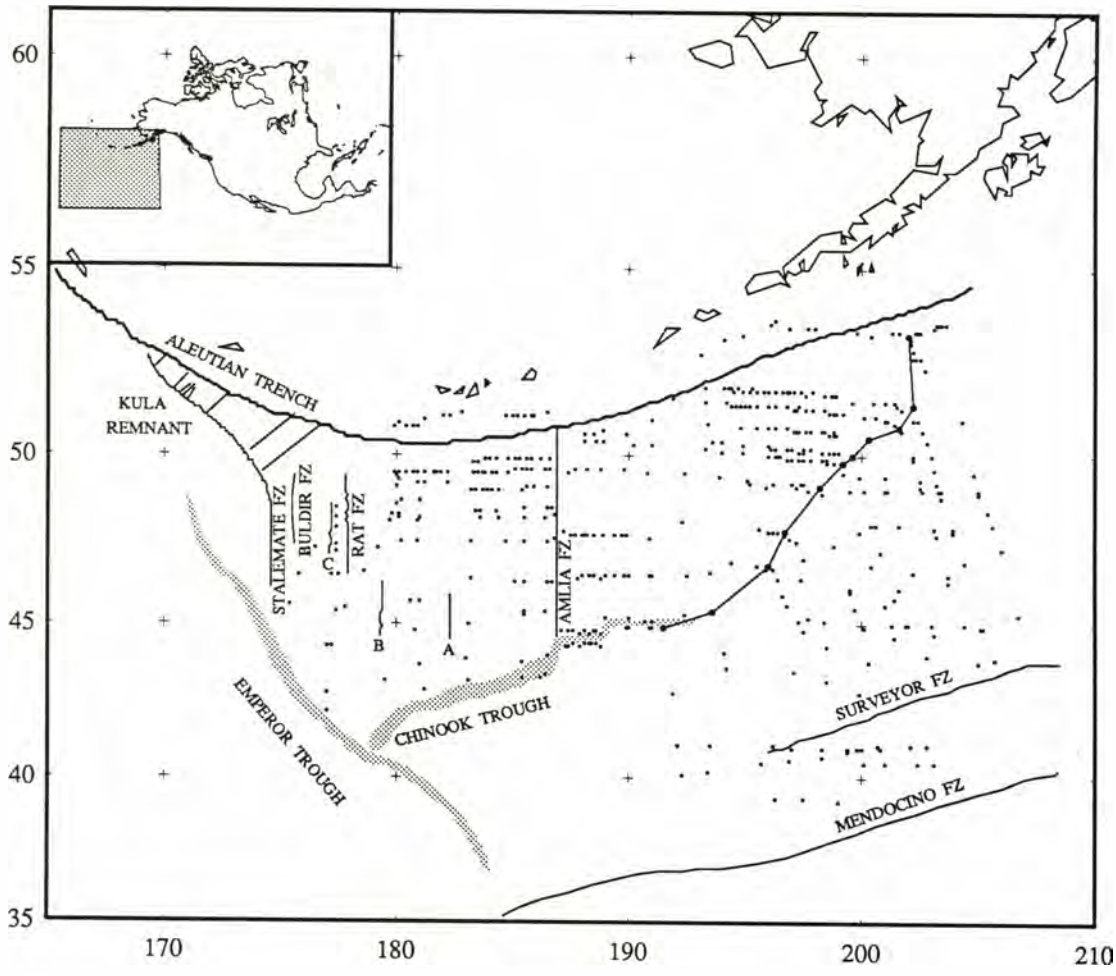

Figure 1. Location map showing study area in the north Pacific. This map and all following maps are Mercator projections. Small dots represent magnetic anomaly picks determined from original ship track data. Large dots connected by lines show the trace of the Pacific-Farallon-Kula triple junction as recorded by the GMB. The Chinook and Emperor Troughs are from Atwater and Severinghaus (1989), and the Aleutian trench is from Chase (1970a). Fracture zone sources are described in Figure 2. The Kula remnant and associated isochrons are after Lonsdale (1988).

that record Pacific to Pacific-Farallon ridge motion were also analyzed and a revised set of their angular rates is presented.

Most chrons identified lie south of the Aleutian Trench, east of the Stalemate Fracture Zone and west of the intersection of the east-west isochrons with the primarily north-south trending chrons of the Pacific-Farallon system. Magnetic chrons near and to the north of the Chinook Trough have been identified as chrons 33 and 34 by Mammerickx and Sharman (1988). Chron 34 is the oldest magnetic isochron of the GMB and defines the northern boundary of the Cretaceous Quiet Zone (Mammerickx and Sharman, 1988). Chron 34 identifications were found on 18 ship tracks and used to constrain Pacific-Kula spreading back to 84 Ma.

The assumption of symmetric crustal accretion across the Pacific-Kula and Pacific-Farallon ridges allows the relative motion poles for the plate-plate rotations to be approximated by those for the plate-ridge rotations, with the rate of angular rotation for the plate being twice that of the ridge. The assumption that seafloor accretion was symmetric across these oceanic ridges was tested by comparing the observed PFK triple junction migration, as recorded by the bend of the GMB (Figure 1), with a predicted triple junction migration based on the updated Pacific-Kula and Pacific-Farallon relative motions presented here.

Previous Work

During the late 1960's and early 1970's, the magnetic chrons of the study area were mapped in varying detail (Peter, 1966; Elvers et al., 1967a, b; Pitman and Hayes, 1968; Hayes and Heirtzler, 1968; Grim and Erickson, 1969; Erickson and

Grim, 1969; Atwater and Menard, 1970; Larson and Pitman, 1972). Elvers et al. (1967b) presented a magnetic-isochron contour map for the northeast Pacific that showed a nearly right angle turn at 50°N, 200°E between north-south and east-west lineation patterns; they named this magnetic structure the "Great Magnetic Bight". The east-west trending isochrons of the GMB were formed at the Pacific-Kula ridge and the northwest-southeast isochrons at the Pacific-Farallon ridge. The "bight" portion of the GMB is bordered on the west by the north-south trending Amlia Fracture Zone at 187°E, and on the south by the Surveyor Fracture Zone which trends 068° between 190°E and 207°E (Rea and Dixon, 1983). Pitman and Hayes (1968) recognized that the east-west trending, northward younging isochrons of the GMB implied the former existence of a now subducted plate. Grow and Atwater (1970) proposed the name "Kula" for this plate, which means "all gone" in an Athabaskan Indian dialect.

The Kula plate began rifting from the Pacific plate during late Cretaceous time. Initial rifting probably occurred at the Chinook Trough (Erickson et al., 1969; Woods and Davies, 1982; Rea and Dixon, 1983). The Chinook Trough, as mapped by Rea and Dixon (1983), is a prominent bathymetric deep with 1500-2000 m of relief located at the southern edge of a 150-200 km wide zone of rough bathymetry (Figure 1). Segments of the Trough are offset left-laterally, similar to the magnetic chrons to the north. At the Amlia Fracture Zone the Trough is offset left-laterally by 130 km (Erickson et al., 1969). The Trough extends from its junction with the Emperor Trough at 41.5°N, 179°E to 45.2°N, 194°E, exactly at the axis of the GMB (Rea and Dixon, 1983). Mammerickx and Sharman (1988) documented a transition from

"rough" to "smooth" bathymetry north of the Chinook Trough and attributed it to a change from relatively slow (< 15 km/my) to fast (> 25 km/my) spreading during chron 33 time (80.17-74.30 Ma). Our analysis of spreading rates is consistent with their findings.

The Kula plate became fused with the Pacific plate sometime in the Eocene when most of the Pacific-Kula ridge would have been far from the Aleutian Trench, leaving the fossil ridge to be subducted. Byrne (1979) argued that, since no west trending chrons north of chron 25 have been identified, the Pacific-Kula ridge must have ceased spreading by chron 24 (55.64 Ma). In the model of Engebretson et al. (1984), the Pacific-Kula ridge continued to spread until about chron 18 (42 Ma). A fossil Pacific-Kula spreading ridge has been identified west of the Rat Fracture Zone (Lonsdale, 1988) in a sizable remnant of Kula plate (Figure 1). The age of this fossil ridge, as determined from magnetic anomaly profiles across the ridge, is 42 Ma and thus the Kula plate is not truly "all gone" (Lonsdale, 1988).

Pole Determination

Pacific-Kula relative motion poles presented here describe Pacific-Kula spreading from 84.00 to 55.64 Ma. Eleven magnetic chrons recording the history of Pacific-Kula spreading (Table 1) define ten time intervals for the following analysis. The goal of this part of the study was to find instantaneous relative-motion poles describing Pacific-Kula spreading and to determine if there were any major changes in pole location or spreading rate. Given the assumption of two pole locations for Pacific-Farallon relative motion between chrons 34 and 24 (Engebretson et al., 1984) an

Table 1. Magnetic chron numbers, ages, and uncertainties.

Chron	Age	l	m	Mean Age (Ma)	Time Spanned (Ma)	Uncertainty (Ma)
34	84.00	1				
			1	82.1	3.83	0.57
33o	80.17	2				
			2	77.2	5.87	0.60
33y	74.30	3				
			3	72.9	2.79	0.33
32a	71.51	4				
			4	70.0	3.04	0.37
30/31	68.47	5				
			5	67.2	2.63	0.15
29	65.84	6				
			6	65.3	1.13	0.26
28	64.71	7				
			7	64.0	1.42	0.33
27	63.29	8				
			8	61.9	2.81	0.64
26	60.48	9				
			9	59.7	1.54	0.35
25	58.94	10				
			10	57.3	3.30	0.28
24	55.64	11				

Note: Eleven possible chron picks (l) yield ten time intervals (m).

updated history of Pacific-Farallon angular rates was also determined. Uncertainties assigned to the input data used to determine the updated Pacific-Kula and Pacific-Farallon relative motion poles were propagated through the entire pole determination process.

Data

Fracture zone azimuths and magnetic chron locations measured along individual ship track segments comprised the data used in the analysis. Thirty-two Pacific-Kula fracture zone azimuths and 88 ship track segments made up of 338 chron locations provided the primary data for the Pacific-Kula kinematic analysis. Pacific-Kula fracture zone locations and orientations were taken from the bathymetric charts of Mammerickx (1989) and the tectonic charts of Atwater and Severinghaus (1989). Forty-six ship track segments consisting of 104 sequential chron locations provided the primary data for the Pacific-Farallon analysis. The original magnetic ship track data sets used were purchased from the National Geophysical Data Center in Boulder, Colorado (Appendices 1 and 2).

Fracture Zone Azimuths

Fracture zones used in the Pacific-Kula analysis were the Amlia, Rat, lower Stalemate, Buldir, and three unnamed Fracture Zones labeled A, B, and C on Figure 2. Best estimates and associated uncertainties in fracture zone azimuths were determined as follows (Figure 3). The bathymetric chart of Mammerickx (1989) and tectonic chart of Atwater and Severinghaus (1989) were superimposed on a light table.

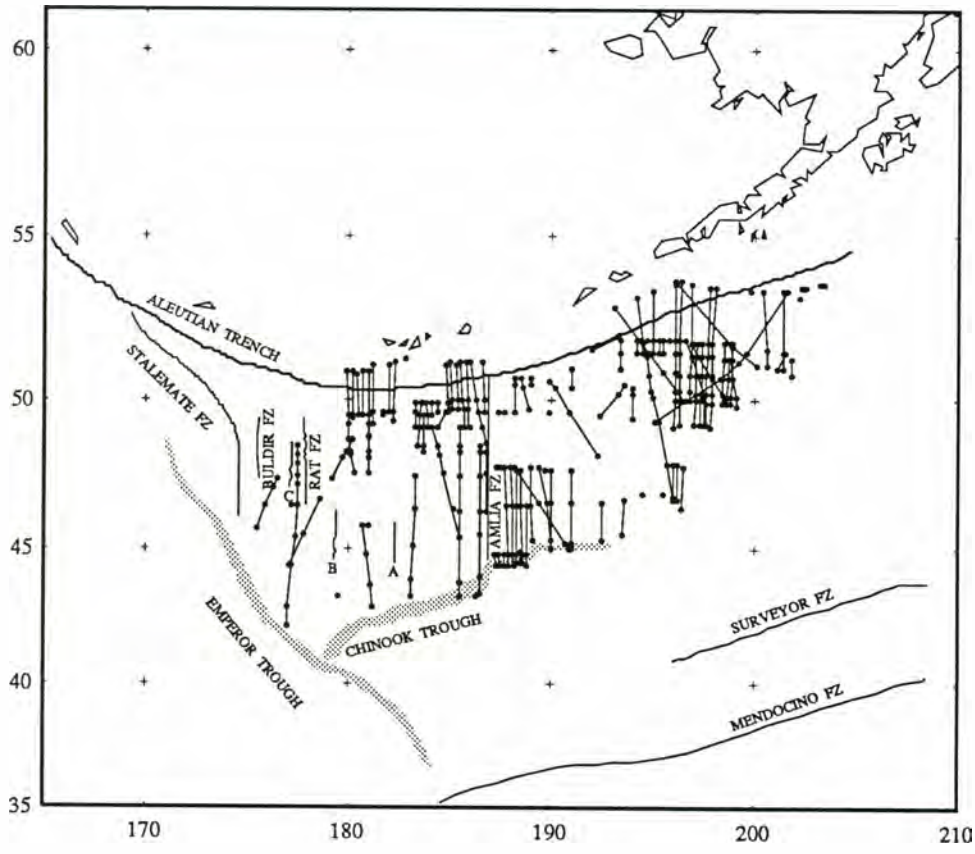

Figure 2. Pacific-Kula fracture zones and ship track segments used in the pole determination. The Amlia Fracture Zone, Stalemate Fracture Zone, and fracture zones labeled A, B, and C are from Atwater and Severinghaus (1989). The Rat and Buldir Fracture Zones are from Mammerickx (1989). Anomaly pairs used to determine angular rates were sequential in both time and space and did not cross fracture zones.

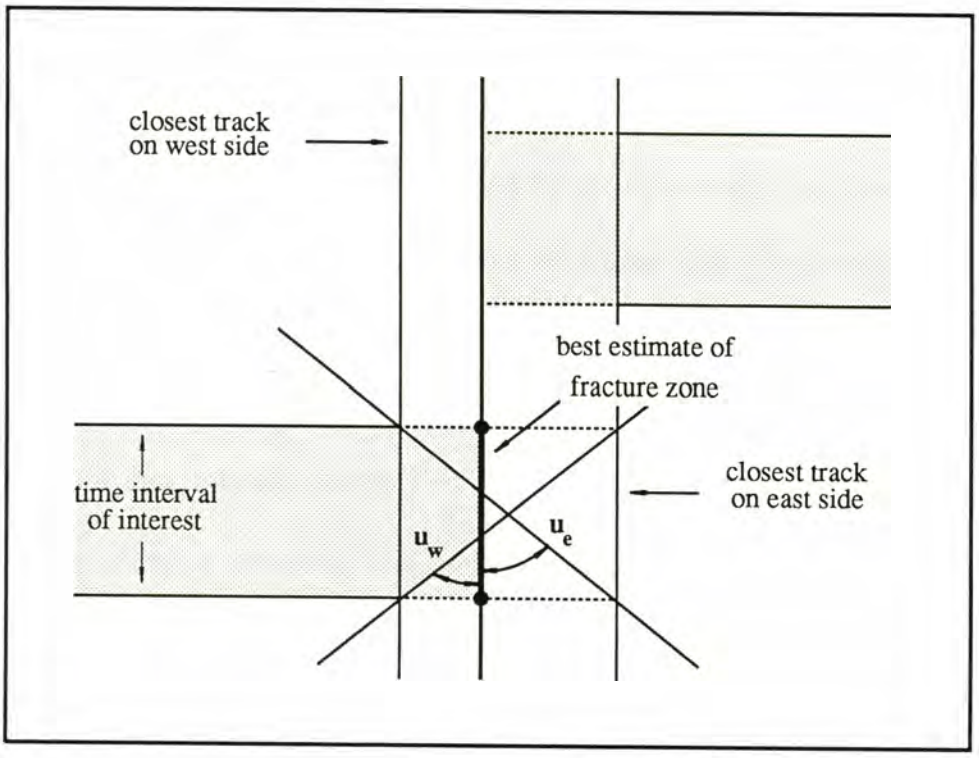

Figure 3. Schematic diagram of method used to assign uncertainties to fracture zone azimuths. Azimuth of thick solid line is the best estimate for the given time interval. Possible departures from the best-fit azimuth are shown by angles u_w and u_e. The largest possible departure was used as $2\,\sigma$ value of azimuthal uncertainty.

Where appropriate, the best estimate of a fracture zone trend within a chosen time interval was obtained by visual inspection of bathymetric contours. Otherwise, trends were chosen directly from the Atwater and Severinghaus (1989) compilation. Maximum allowable departures from this best azimuthal estimate correspond to great circle segments that lie within a region bounded by the closest ship tracks on either side of the fracture zone (Figure 3). Local azimuths of great circle segments drawn along diagonals through the region were calculated and the largest departure was chosen as the 2σ estimate of uncertainty. Table 2 contains the azimuths of the 32 fracture zone trends used and their related uncertainties.

Because of these geometric constraints, time intervals with short time spans tended to have large azimuthal uncertainties. The southernmost segment of the Amlia Fracture Zone, which constrains the oldest Pacific-Kula relative motion (from chron 34 to chron 33o), has very little azimuthal control. The intersection of the Amlia Fracture Zone with the Chinook Trough obscures the bathymetric interpretation of this segment. Slow spreading during this time interval resulted in rough bathymetry in this region (Mammerickx and Sharman, 1988), and ship track magnetics can not be used due to infrequent reversals. The estimated azimuth of this oldest Pacific-Kula segment was constrained by the chron 34 and 33o designations on the tectonic map of Atwater and Severinghaus (1989). The Amlia Fracture Zone provides the only control on the azimuth and uncertainty for time interval 2 (Table 1). The best estimated azimuth for this time interval was determined from bathymetric contours; the uncertainties are small due to the proximity of bounding ship tracks and the relatively long time spanned during the normal polarity interval (5.87 my). Azimuthal data for time

Table 2. Fracture zone azimuths and uncertainties

Chron		Latitude	Longitude	Azimuth	Uncertainty
From	To	°N	°E	°E	(deg)
34	33o	43.9	186.9	186.5	28.5
33o	33y	45.6	186.9	181.2	10.3
33o	33y	44.7	186.9	181.5	14.3
33y	32a	47.2	187.0	179.9	11.0
33y	32a	45.9	186.9	180.3	16.3
33y	32a	45.5	182.3	179.1	14.9
33y	32a	45.2	179.3	180.9	28.2
32a	30/31	48.8	186.9	178.0	7.8
32a	30/31	46.9	186.9	180.3	13.3
30/31	29	50.1	186.9	180.0	10.5
30/31	29	47.9	186.9	177.8	15.9
30/31	29	46.8	174.6	178.8	31.8
29	28	48.5	186.9	173.0	33.1
29	28	47.4	177.6	177.9	26.7
29	28	47.3	177.1	179.7	24.1
29	28	48.1	177.6	180.2	26.8
28	27	48.9	186.9	179.7	19.6
28	27	47.7	177.6	179.0	24.6
28	27	47.6	177.1	180.0	19.3
28	27	48.5	177.6	182.5	25.2
28	27	47.6	175.6	180.9	38.4
27	26	49.4	186.9	180.6	19.2
27	26	48.1	177.6	180.1	28.4
27	26	47.9	177.1	179.4	25.3
27	26	48.8	177.6	185.7	25.6
27	26	48.0	175.5	177.1	39.7
26	25	49.8	186.9	181.4	21.5
26	25	48.4	177.6	181.2	25.1
26	25	48.2	177.2	180.0	27.2
26	25	49.1	177.7	179.9	26.2
26	25	48.2	175.5	179.6	40.7
25	24	49.6	177.7	179.9	15.1

Notes: Latitude and longitude represent the center of the fracture zone segment. Azimuthal uncertainty represents 1σ.

interval 3 are controlled by the Amlia Fracture Zone and Fracture Zones A and B (Figure 2). Wide ship track spacing defining the offset of chron 32 results in an uncertainty of 28.2 degrees for Fracture Zone B (Table 2). Time interval 4 was tightly controlled by ship tracks adjacent to the Amlia Fracture Zone. Intervals 5 through 9 were constrained by the Amlia Fracture Zone, Rat Fracture Zone, and Fracture Zone C. In all intervals, the best estimated azimuth of the Rat Fracture Zone was obtained from bathymetric contours. Azimuthal uncertainty for interval 10 was constrained only by ship tracks adjacent to the Rat Fracture Zone.

Magnetic Chron Locations

Anomaly identifications were made by plotting observed magnetic anomaly profiles (the residual magnetic field versus distance along ship tracks) and comparing their shape, amplitude, and spacing to the worldwide sequence of polarity reversals. When plotting the observed profiles, the residual field strengths given in the NGDC's data set were used. Following anomaly identification, corresponding chron locations were assigned in the form of chron number, latitude, and longitude. Chrons 24 through 29 and chron 32a were located at the center of the given normally-magnetized crustal block. Chron 30/31 was located at the center of the short reversal between the normals of 30 and 31. Chrons 33y, 33o, and 34 were located at the spatial edge of the normally magnetized blocks (Figure 4a). Chron ages were assigned using the polarity reversal timescale of Berggren et al. (1985).

To aid in chron identification, synthetic anomaly profiles were generated to match the observed anomaly profiles. The upper curves in Figure 4a represent an

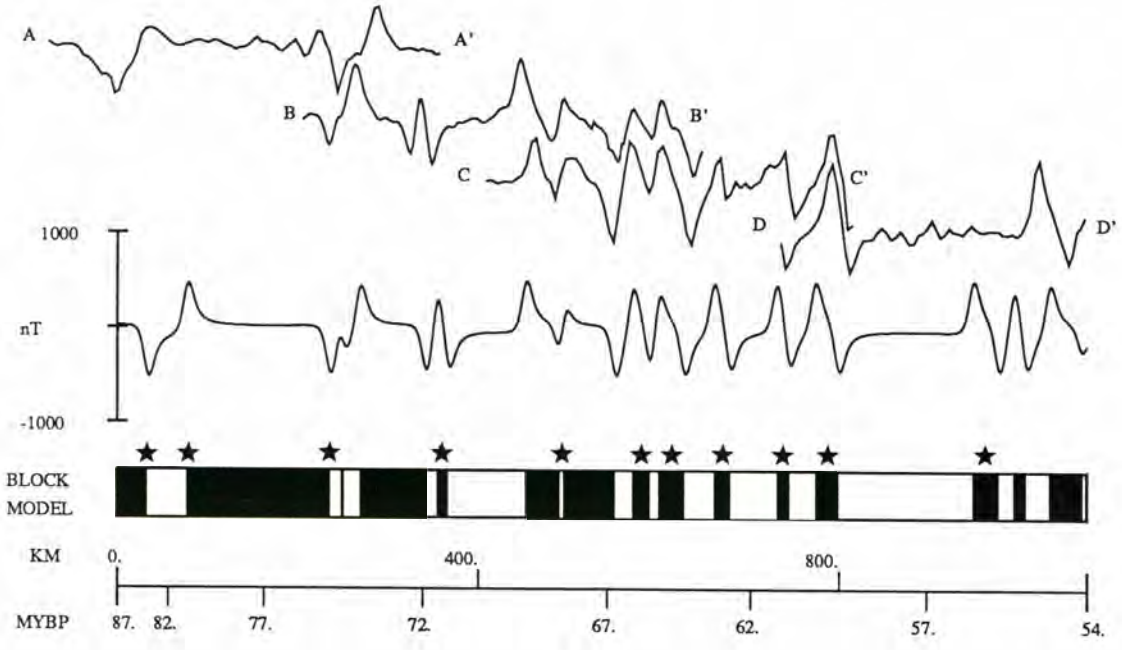

(a)

Figure 4. (a) Synthetic anomaly profile (lower curve) compared with composite magnetic profiles (upper curves) from lines A-A' through D-D' shown in Figure 4b. The parameters of the magnetic block model are: distance to top of layer = 5.0 km; distance to bottom of layer = 5.5 km; magnetic dipole moment per unit volume = 18 A/m (conversion from emu after Shive, 1986); remanent declination = 20°E; remanent inclination = 45° (corresponding to approximate paleolatitude during formation) ; ambient declination = 20°E; ambient inclination = 67°; spreading azimuth was assumed to be north-south; polarity transition filter with 2 σ width of 3.0 km. Stars represent locations of anomaly identifications used in this study.

(b) Location of magnetic profiles A-A' through D-D' used to construct the composite profile shown in Figure 4a.

(c) Half-spreading velocities and associated 1 σ uncertainties used in the construction of the model anomaly profile shown in Figure 4a. Linear velocities for time intervals 1 through 10 were determined at points along profiles A-A' through D-D' shown in Figure 4b. The number of sequential anomaly pairs along ship tracks used to calculate the model velocity are shown near each time interval.

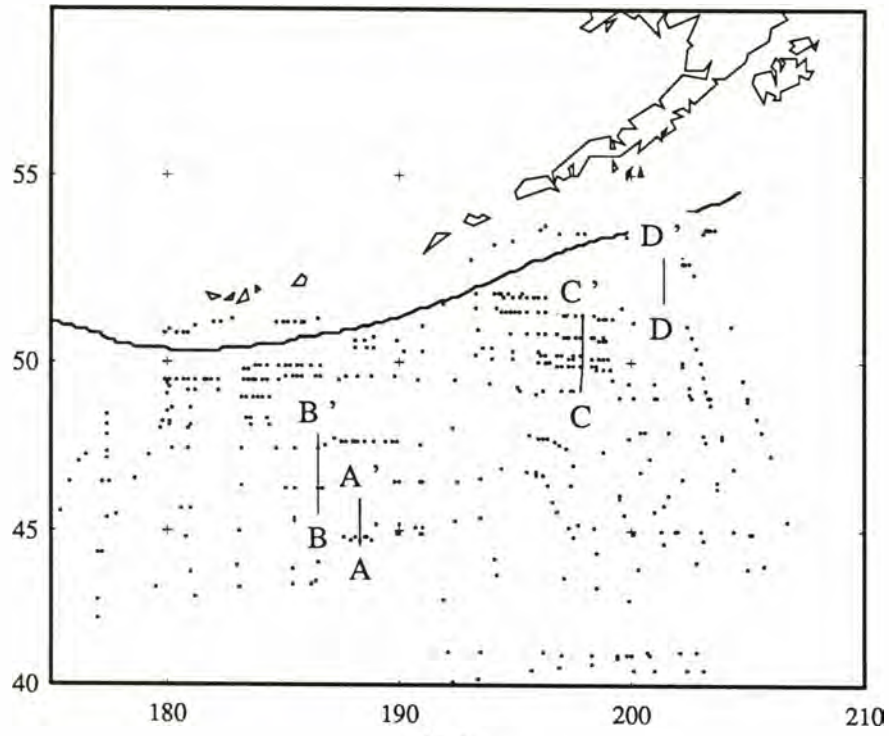
55
50
45
40
180
190
200
210
D '
C '
D
C
B '
A '
B
A

(b)

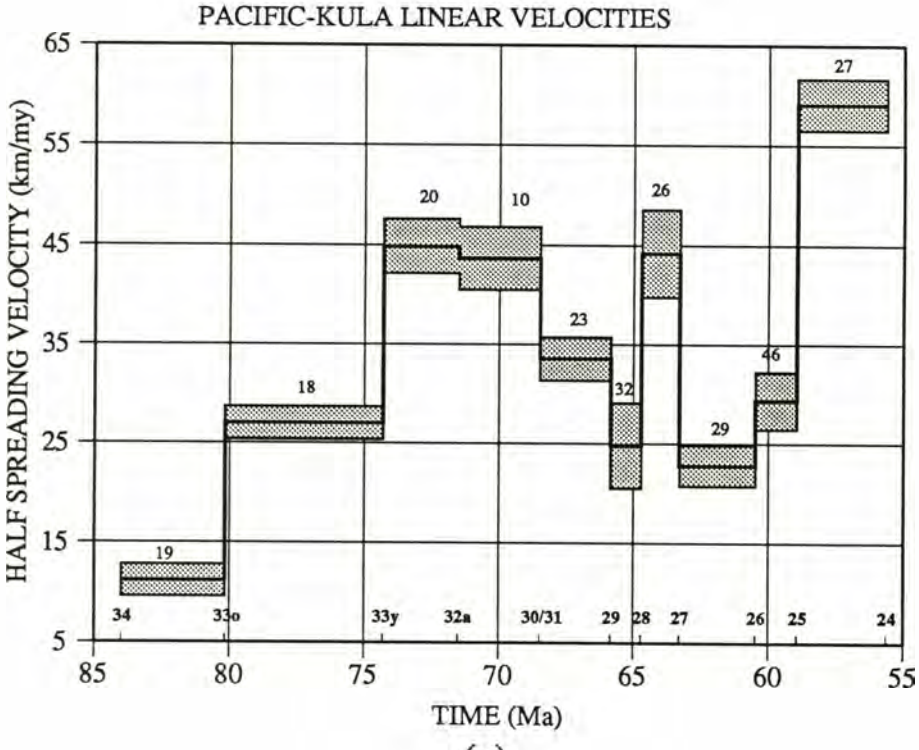
PACIFIC-KULA LINEAR VELOCITIES
HALF SPREADING VELOCITY (km/my)
65
55
45
35
25
15
5
85
80
75
70
65
60
55
TIME (Ma)
19
18
20
10
23
32
26
29
46
27
34
33o
33y
32a
30/31
29
28
27
26
25
24

(c)

observed composite profile along the lines A-A' through D-D', shown in Figure 4b. The lower curve in Figure 4a is a synthetic profile modeled in terms of alternately magnetized vertical blocks. Parameters used to generate the models are given in the caption of Figure 4. Where observed profiles did not cross fracture zones or pseudofaults, identification of individual chrons was straightforward (Figure 4a). The oldest chrons (34 and 33o) and the youngest chrons (25 and 24) of the Pacific-Kula sequence had the largest variation in shape when compared to model profiles.

Uncertainties were assigned to the chron locations using the following reasoning. The amplitude of magnetic 'noise' on the ship track anomaly profiles was estimated to be approximately 100nT. The effect of adding or removing 100nT from the amplitude of each side of an anomaly is to give an uncertainty in that chron location of approximately 15 km. An uncertainty of 10 km was also assigned to chron locations due to possible ship navigation errors. A corresponding RMS uncertainty of 18 km was assigned to chron locations assuming these two sources of error are not correlated.

Systematic errors in chron location picks which result from anomalous skewness in the observed Pacific-Kula anomaly profiles have been ignored in this work. Petronotis and Gordon (1989) found that skewness differs significantly between adjacent Pacific-Kula chrons. In future work, values of skewness could be assigned to each Pacific-Kula anomaly based on estimates for anomalous skewness provided by Petronotis and Gordon (1989). Spreading rates determined between adjacent chrons could then be determined taking into account the systematic errors induced by anomalous skewness, resulting in a more precise Pacific-Kula spreading history.

Uncertainties were assigned to the times spanned between chrons by comparing the time scale used in this study (Berggren et al., 1985) with the time scale of Harland et al. (1982). The difference between time spanned through consecutive chron intervals was determined for each time scale, and used as the estimated 1 σ uncertainty in the length of that given time interval (Table 1).

Most of the mapped chron pattern of the GMB is similar to those of previous workers (Figure 1). Chron 34 was identified north of the Chinook Trough along its entire length. These identifications agree with Mammerickx and Sharman (1988), but those to the east of the Amlia Fracture Zone are not shown on the tectonic charts of Atwater and Severinghaus (1989). In this work, chron 24 was identified north of the Aleutian Trench between 180°E and 187°E. These identifications have not been included on previous compilations.

Methods

Several methods have been developed to obtain "best-fitting" relative motion poles. Some are based on determining finite rotations (total reconstructions or stage poles) and their associated uncertainties. Molnar and Stock (1985) assigned uncertainties to finite rotations by deriving three "partial-uncertainty" rotations that could be added to and subtracted from the best-fit finite rotation. Commonly, these poles cover time intervals of several millions of years and are specific to only a few magnetic chrons. These finite rotations necessarily represent motions that are averaged over time intervals which may have contained significant changes in pole position or rates.

Other methods use instantaneous relative motion vectors that are often found using a least-squares approach (e.g. Chase, 1972; Minster et al., 1974; Engebretson et al., 1984; DeMets et al., 1990). Uncertainties for these analyses are represented by regions surrounding the best-fit pole where acceptable poles have been located, and have tolerance limits on an angular rate. An advantage of this approach is that shorter intervals of time can be studied providing a greater opportunity to decipher possible pole location changes and variations in angular rates. These instantaneous poles are extended to finite rotations by multiplying the angular rates by the appropriate time spanned by the data.

Chi-Square

This study employed a method to find instantaneous vectors that minimizes a total squared error (chi-square) by weighting an individual datum according to its assigned uncertainty. An important advantage of this treatment is that contributions from dimensionally disparate data can be combined. The approach developed here was chosen in order to check if there were significant changes in either the position or angular rate of the relative motion poles. As discussed later, there were at least two changes in Pacific-Kula pole position, and several changes in angular rate during a time of nearly constant pole position.

Contributions to the chi-square come from two data types - fracture zone azimuths and pairs of successive magnetic chrons along ship tracks (resulting in estimates for angular velocity). Fracture zone azimuths provide an estimate of the direction of relative plate movement and thus help constrain the pole location. Pairs of

magnetic chrons provide constraints on angular rates but also influence pole location since there is no dependence of angular rate with colatitude from the poles. Therefore the angle subtended at the pole by any pair of chrons spanning the same time should be the same along the entire plate boundary. It should be noted that if there existed departures from orthogonality of transforms and ridges, ship tracks that are not parallel to flow lines could provide estimates in error of the true angular velocity. However, the majority of the ship tracks used in this analysis are nearly parallel to fracture zones (flow lines) and it is clear by inspection that spreading has been nearly orthogonal.

For each time interval or series of time intervals the best-fitting pole was found by minimizing the total squared error:

$$\chi^2 = \sum_{i=1}^{L} \left[\sum_{j=1}^{M_i} \left[\frac{\overline{\omega}_i - \omega_{i\,j}}{\sigma_{i\,j}} \right]^2 + \sum_{k=1}^{N_i} \left[\frac{\cos^{-1}\left[\hat{a}_m \cdot \hat{f}_{i\,k}\right]}{\sigma_{i\,k}} \right]^2 \right].$$

For any series of L time intervals, the total error was found by summing the weighted misfits of $\sum M_i$ angular rates and $\sum N_i$ fracture zone azimuths. For $\sum M_i$, $\overline{\omega}_i$ represents the average angular rate within the i^{th} time interval;

$\overline{\omega}_i = \frac{1}{M_i} \sum_{j=1}^{M_i} \omega_{i\,j}$, with $\omega_{i\,j} = \frac{\Omega_{i\,j}}{t_0 - t_1}$. Here $\omega_{i\,j}$ is the j^{th} angular rate (see Figure 5) that lies within the i^{th} time interval (between times $t_0 - t_1$) and has the assigned uncertainty $\sigma_{i\,j}$. For $\sum N_i$, $\hat{a}_m$ is the model unit vector obtained from the trial pole, $\hat{t}$ (Figure 5), i.e. $\hat{a}_m = \frac{\hat{t} \times \hat{r}}{|\hat{t} \times \hat{r}|}$. Here $\hat{f}_{i\,k}$ is the k^{th} observed fracture zone azimuth that lies within the i^{th} time interval and has the assigned uncertainty

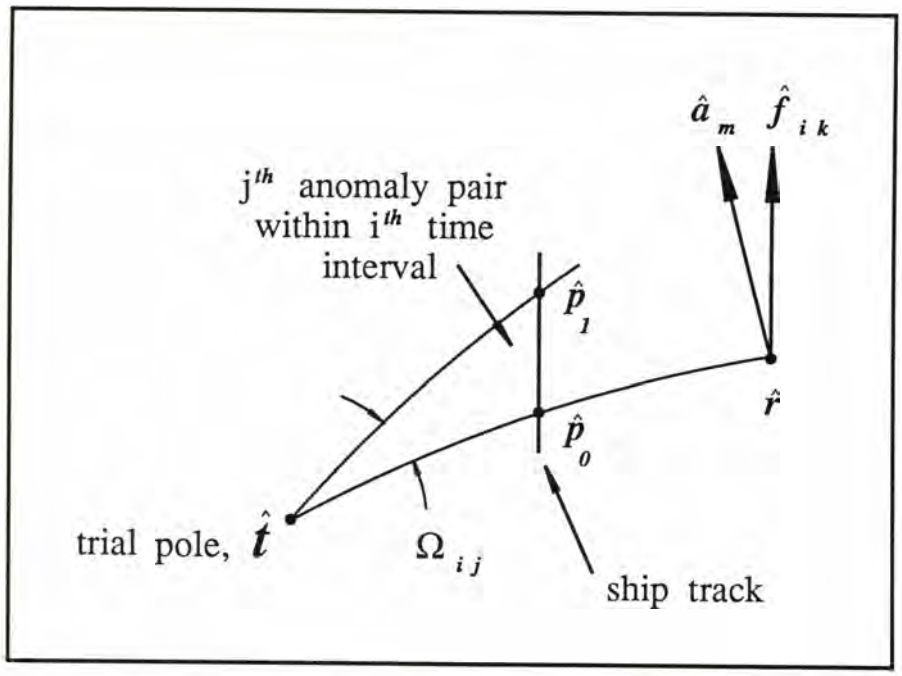

Figure 5. Schematic diagram of fitting functions used in the chi-square method. $\hat{p}_0$ and $\hat{p}_1$ are positions of anomaly picks for times t_0 and t_1 respectively. Ω_{ij} is the angle subtended at $\hat{t}$ by $\hat{p}_0$ and $\hat{p}_1$, thus $\omega_{ij} = \Omega\frac{ij}{t_0 - t_1}$ is the measured angular velocity for this pair. $\hat{a}_m$ is the unit vector at position $\hat{r}$ perpendicular to the great circle between $\hat{t}$ and $\hat{r}$. Here $\hat{f}_{ik}$ is the k^{th} observed fracture zone that lies within the i^{th} time interval. See text for further discussion.

$\sigma_{i\,k}$. Note that the total number of adjustable parameters with this fitting function is $L + 2$, that is, L adjustable angular rates, $\omega_{i\,j}$, and two additional parameters for the latitude and longitude of the best-fit pole.

A search technique was applied by determining a 9 by 9 grid of trial poles centered on a chosen pole. The search for a time interval (or multiple time intervals) began with a 10 degree grid spacing. The center of the grid was changed until a best-fit pole (minimum χ^2 within the central portion of the grid) was isolated. This procedure was repeated with incrementally reduced grid spacings until the pole was found to within 0.5 degrees. No local minima were encountered using this approach.

Confidence Intervals

To estimate confidence intervals, measurement errors were assumed to be normally distributed and were analyzed by linear approximations. Contours of $\Delta\,\chi^2$ for a 1 σ level of confidence were constructed as follows (see Bevington, 1969; Press et al., 1986). Let $\Delta\,\chi^2 = \chi^2_\nu - \chi^2_{\min}$ where $\chi^2_{\min}$ is the minimum value of χ^2 found by the search method explained earlier and corresponds to a fitting function with ν adjustable parameters. χ^2_ν are values of χ^2 found by alternative choices of the ν parameters. In this study $\nu = L + 2$ since there are L estimates of angular rates plus a latitude and longitude. In practice, 1 σ confidence intervals were chosen by perturbing the pole at small increments away from the best-fit latitude and longitude (readjusting the L angular rates to minimize χ^2) until $\Delta\,\chi^2$ exceeded critical values found for ν degrees of freedom.

For example, for a single time interval, the region surrounding the best-fit pole

bounded by a constant $\Delta \chi^2$ value of 3.53 (3 degrees of freedom) was determined. Further, for 1 σ confidence intervals on the angular rates at the best-fit pole, the best-fit rate was perturbed by adding and subtracting small (.001 deg/my) increments until $\Delta \chi^2$ exceeded 1.0 (1 degree of freedom). End-member poles describing each confidence region were based on the point on the bounding region located farthest from the best-fit pole. The 3 remaining end-member poles were located approximately 90°, 180°, and 270° in azimuth away from that location along the bounding region.

Results

Pacific-Kula

The final product of the Pacific-Kula relative motion pole analysis is presented in Table 3 as a set of ten stage poles, each describing the motion of the Kula plate relative to a fixed Pacific plate. These ten stage poles are defined by three pole locations and ten angular rates and their corresponding finite angles. Rotation conventions are that the Pacific plate remains fixed and the rotation of the Kula plate during a given time interval is described forward in time. The first line in Table 3 describes the rotation of the Kula plate (as seen by an observer on the Pacific plate) from its position at chron 34 (84.00 Ma) to that at chron 33o (80.17 Ma). The amount of angular rotation for this time interval is 6.19°. End-member poles for the Pacific-Kula confidence regions found using the chi-square technique described earlier are listed in Table 4. Total reconstruction poles describing the rotation necessary to restore the Kula plate to its position relative to the Pacific plate at various times between chron 24 and 34

Table 3. Pacific-Kula Stage Poles

Chron		Latitude	Longitude	Finite Angle	Whole-Rates (deg/my)		
From	To	°N	°E	(deg)	Best	Maximum	Minimum
34	33o	- 44.1	18.0	6.19	1.615	1.847	1.433
33o	33y	29.3	125.2	3.67	0.626	0.646	0.588
33y	32a	29.3	125.2	2.93	1.051	1.097	0.987
32a	30/31	29.3	125.2	3.11	1.023	1.097	0.949
30/31	29	29.3	125.2	1.89	0.719	0.765	0.673
29	28	29.3	125.2	0.60	0.531	0.623	0.441
28	27	29.3	125.2	1.34	0.946	1.032	0.852
27	26	29.3	125.2	1.37	0.488	0.532	0.448
26	25	29.3	125.2	0.97	0.629	0.691	0.575
25	24	37.3	149.4	5.12	1.708	1.754	1.804

Note: The Pacific plate remains fixed and the rotation of the Kula plate during the time spanned by a pair of chrons is described going forward in time (right hand rule).

Table 4. Pacific-Kula end-member poles

Chron		Latitude	Longitude	Whole Rate
From	To	°N	°E	(deg/my)
34	33o	-43.3	12.0	2.837
34	33o	-44.4	40.1	0.539
34	33o	-49.3	16.7	1.19
34	33o	-39.3	19.	1.042
33o	33y	-10.4	84.3	0.508
33o	33y	41.8	149.6	1.049
33o	33y	24.3	129.6	0.629
33o	33y	34.3	120.2	0.603
33y	32a	-10.4	84.3	0.852
33y	32a	41.8	149.6	1.778
33y	32a	24.3	129.6	1.052
33y	32a	34.3	120.2	1.018
32a	30/31	-10.4	84.3	0.790
32a	30/31	41.8	149.6	1.824
32a	30/31	24.3	129.6	1.010
32a	30/31	34.3	120.2	1.001
30/31	29	-10.4	84.3	0.594
30/31	29	41.8	149.6	1.196
30/31	29	24.3	129.6	0.703
30/31	29	34.3	120.2	0.713
29	28	-10.4	84.3	0.447
29	28	41.8	149.6	0.867
29	28	24.3	129.6	0.524
29	28	34.3	120.2	0.523
28	27	-10.4	84.3	0.798
28	27	41.8	149.6	1.538
28	27	24.3	129.6	0.939
28	27	34.3	120.2	0.927
27	26	-10.4	84.3	0.412
27	26	41.8	149.6	0.789
27	26	24.3	129.6	0.485
27	26	34.3	120.2	0.478
26	25	-10.4	84.3	0.530
26	25	41.8	149.6	1.015
26	25	24.3	129.6	0.621
26	25	34.3	120.2	0.619
25	24	29.	130.4	1.191
25	24	40.5	162.0	2.327
25	24	32.0	151.9	1.534
25	24	43.4	146.0	1.804

Table 5. Total reconstruction poles for the Kula plate relative to a fixed Pacific plate

Chron	Age (Ma)	Latitude °N	Longitude °E	Angle (deg)
24	55.64	-	-	0.00
25	58.94	- 37.3	329.4	5.12
26	60.48	- 36.2	325.4	6.03
27	63.29	- 35.0	321.5	7.35
28	64.71	- 34.2	318.9	8.65
29	65.84	- 33.8	318.0	9.23
30/31	68.47	- 33.0	315.8	11.09
32a	71.51	- 32.1	313.5	14.17
33y	74.30	- 31.5	312.1	17.07
33o	80.17	- 31.0	311.0	20.72
34	84.00	- 18.9	298.8	17.72

Note: Total reconstruction poles relative to a fixed Pacific plate describing the rotation necessary to restore the Kula plate from its position at the time of chron 24 (55.64 Ma) to its former positions at times given in the second column.

are shown in Table 5.

Individual instantaneous Pacific-Kula relative motion poles originally determined for each of the ten time intervals appear to migrate through time (Figure 6a). A large jump apparently occurred between the end of time interval 1 and the end of time interval 2. Pole migration probably continued through time intervals 3 and 4. Migration, if any, was small during intervals 5 through 9 with a moderate amount seen between 9 and 10. Uncertainties inherent in the data preclude derivation of 10 significantly different poles along this apparent pole migration path. As mentioned above and dicussed below, three pole locations with associated confidence regions adequately describe Pacific-Kula relative motions (Figure 7).

Time interval 1 can be modeled as a distinct instantaneous relative motion pole describing Pacific-Kula motion from chron 34 to 33o (Figure 6b). A significant pole migration cannot be distinguished between time intervals 2 through 10 at the 1 σ confidence level (Figure 6b). Based on the confidence regions for time intervals 2 through 9, a single pole location adequately describes Pacific-Kula relative motion from chron 33o through chron 25. Although not distinct from poles for intervals 2-9 on this basis, the relative motion pole describing Pacific-Kula motion from chron 25 to 24 (time interval 10) was modeled as a distinct pole based on the following reasoning. 1) The shape of the confidence region constraining this stage pole is different than the shape of the confidence regions constraining poles for time intervals 2 through 9. 2) The pole location for time interval 10 lies outside of the interval 2-9 confidence region and vice versa (Figure 7). 3) Previous workers have noted a major reorganization of the Pacific-Kula ridge system at or soon after chron 25 (Atwater and

Figure 6. (a) Ten Pacific-Kula instantaneous relative motion poles originally determined from the data. These poles show a general migration in pole location over time. Note that the antipole for time interval 1 is located just to the east of the GMB.

(b) The same pole locations as in Figure 6a are shown with their associated 1σ confidence regions. Only interval 1 appears to have a significantly different pole location.

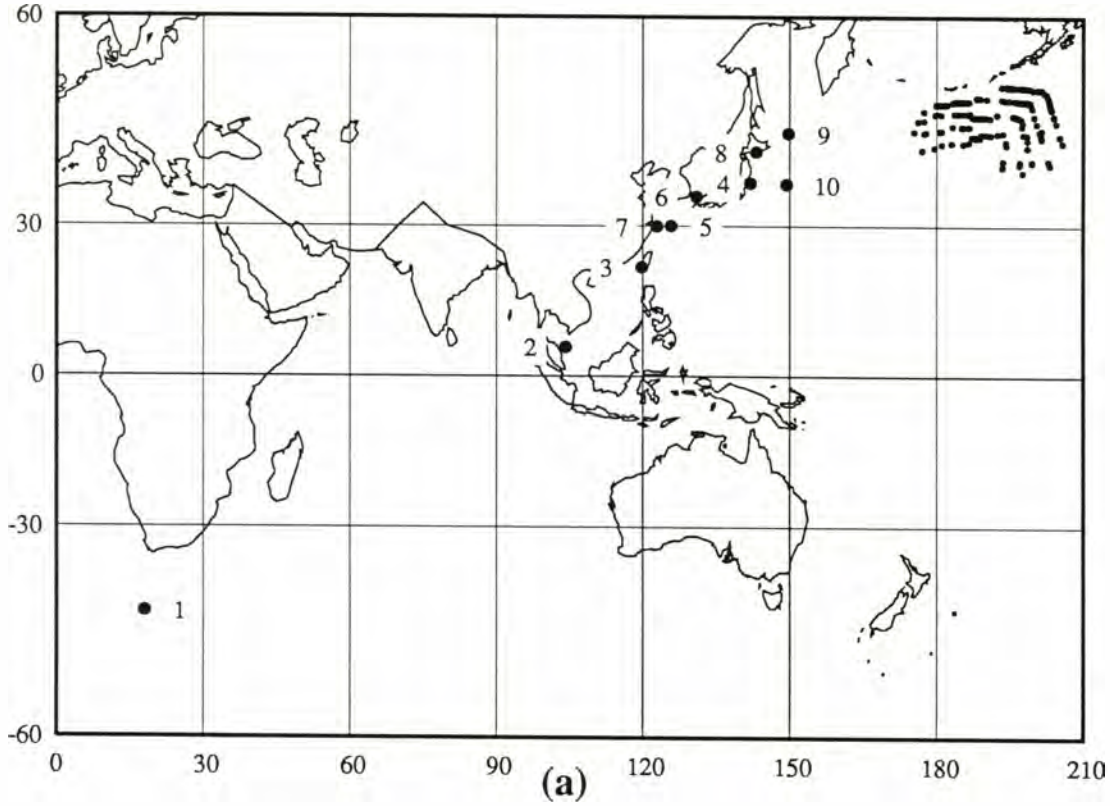
60
30
0
-30
-60
0
30
60
90
120
150
180
210
1
2
3
4
5
6
7
8
9
10

(a)

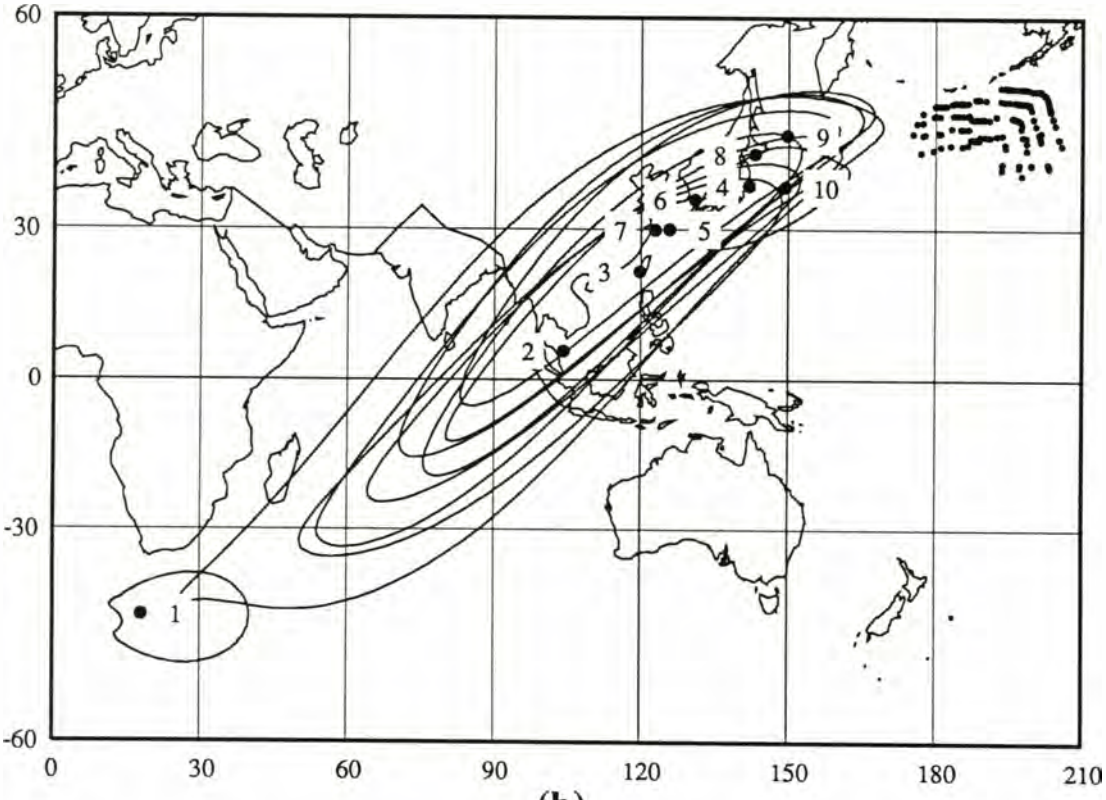
60
30
0
-30
-60
0
30
60
90
120
150
180
210
1
2
3
4
5
6
7
8
9
10

(b)

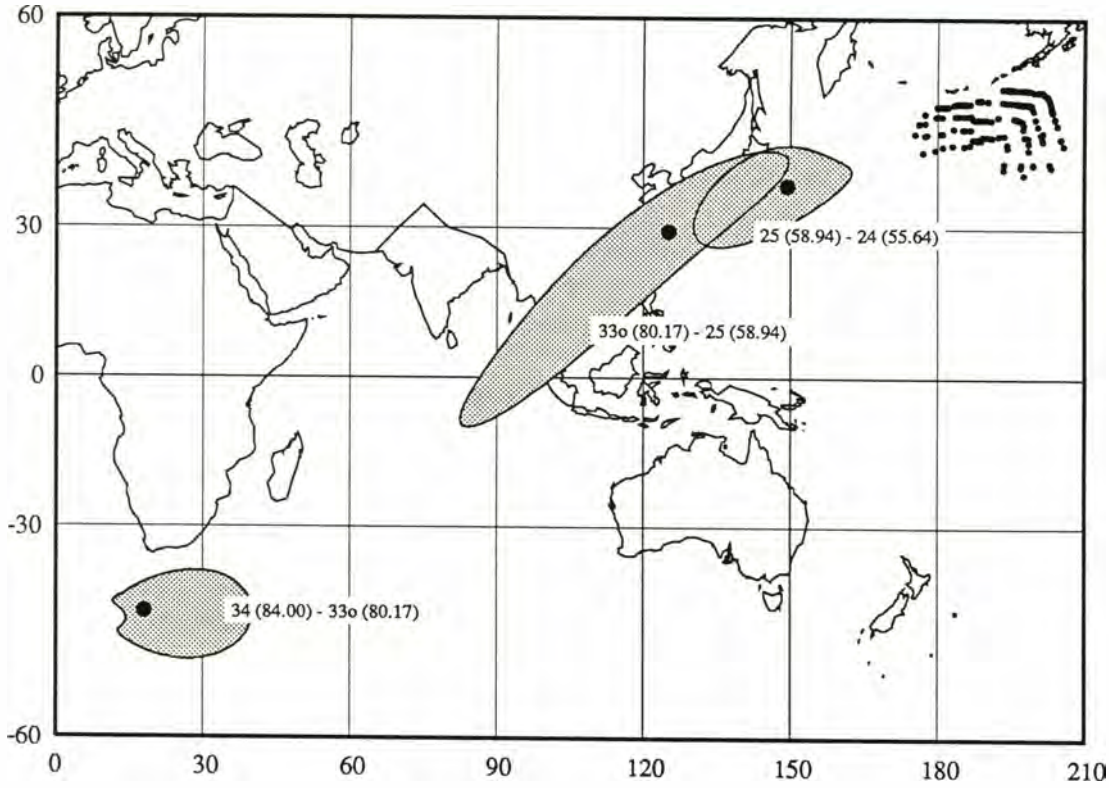

Figure 7. Updated Pacific-Kula instantaneous relative motion pole locations and confidence regions. Dots within shaded confidence regions represent the best-fit stage pole for the time intervals shown. Black dots in upper right represent anomaly picks which partially describe the Great Magnetic Bight.

Menard, 1970; Engebretson et al., 1984; Lonsdale, 1988; and Rosa and Molnar, 1988). 4) The Pacific-Kula spreading rate during this time increased markedly (Figure 8).

Pacific-Kula linear velocities were determined for each of the ten stage poles shown in Table 3. Pacific-Kula (and Pacific-Farallon) linear velocities were determined at the apex of the GMB at the intersection of the oldest Pacific-Kula and Pacific-Farallon isochron defining a given time interval in order to facilitate the analysis that follows in a later section, which investigates the PFK triple junction migration. Pacific-Kula linear velocities determined along the GMB for the 10 time intervals are shown in Figure 8. It should be noted that the antipole for time interval 1 (Figure 7) is located just east of the GMB, which accounts for the high angular rate (Table 3) but low linear velocities (Figure 8) of this time interval.

Pacific-Farallon

Stage poles describing the relative motions between the Pacific plate and the Pacific-Farallon ridge were updated by re-evaluating Pacific-Farallon spreading rates through analysis of the Pacific-Farallon magnetic chrons near the GMB. This allowed for a comparison of Pacific-Kula and Pacific-Farallon spreading velocities at the triple junction for each time interval. Relative motion pole locations and associated end-member locations were taken from Engebretson et al. (1984). Use of these poles can be justified on the basis that the fracture zone data set used by Engebretson et al. (1984) extended from the Gulf of Alaska to the southern Pacific and that a single Farallon plate existed throughout this region (Engebretson et. al, 1984; Rosa and Mol-

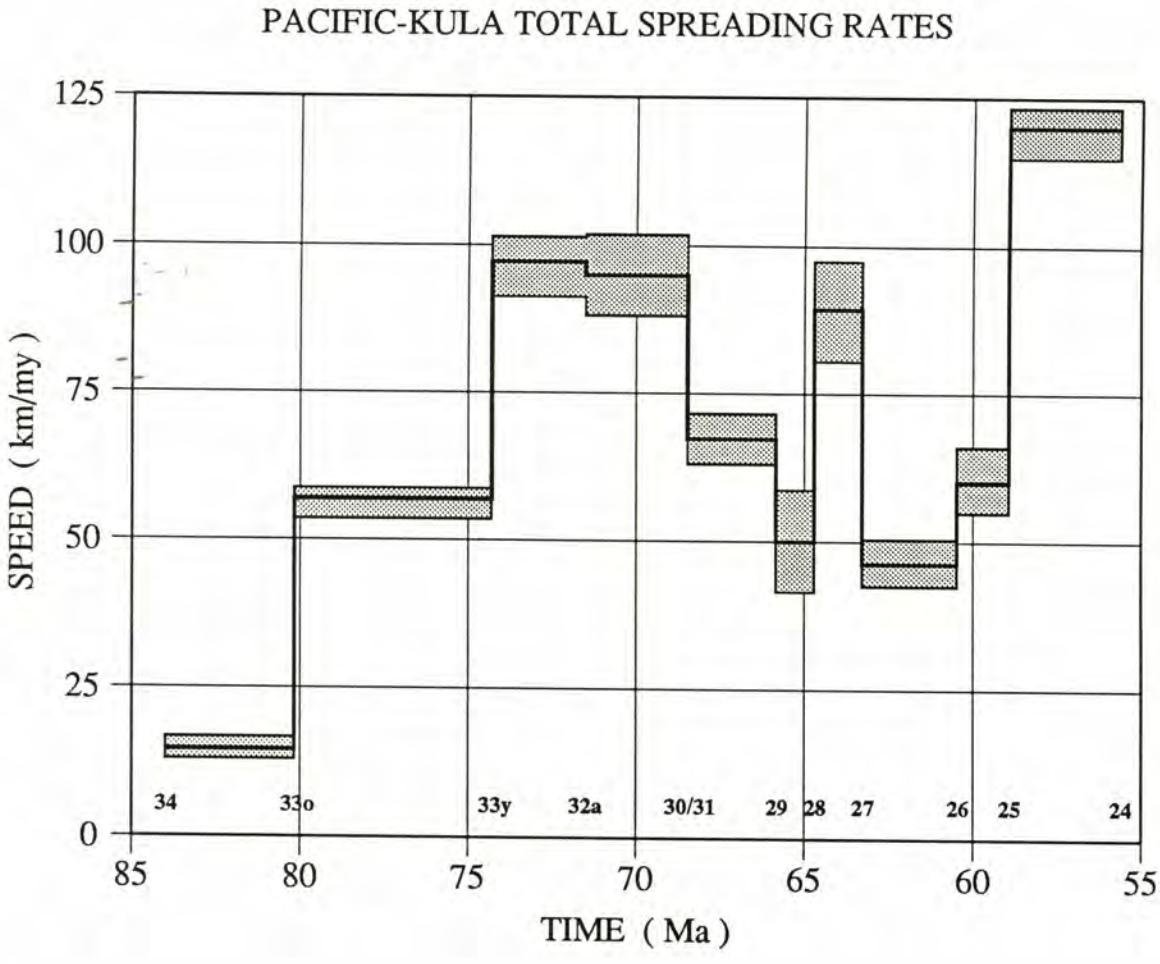

Figure 8. Pacific-Kula linear velocities determined at the apexes of the GMB. Central black line represents the best-fit linear velocity for each of the time periods shown. Shaded regions show 1 σ uncertainties for the best-fit linear velocities.

nar, 1988).

Pacific-Farallon angular rates were updated by analyzing 46 ship tracks consisting of 104 sequential chron identifications. Updated Pacific-Farallon stage poles for the 10 time intervals are shown in Table 6. Pacific-Farallon confidence region end-member poles are listed in Table 7. Pacific-Farallon linear velocities determined at the apex of the GMB are shown in Figure 9.

Interpretation

Pacific-Kula relative-motion poles presented here quantitatively agree with those of previous workers (Figure 10). Engebretson et al. (1984) and Rosa and Molnar (1988) determined Pacific-Kula relative motions for the time interval between chrons 32 and 25. The confidence region presented here for this time interval includes their pole locations. Lonsdale (1988) determined a Pacific-Kula pole for the time interval between chrons 23 and 21 based on data to the west of the study area. The confidence region constraining the chron 25 to 24 time interval pole includes this pole location (Figure 10). It is interesting to note that the chron 23 to 21 pole of Lonsdale (1988) lies along the migration path discussed earlier in the text.

Results of the kinematic analysis (Table 3) describe a sporadic history of Pacific-Kula spreading with two pole location changes (Figure 7) and numerous velocity changes (Figure 8). Initiation of Pacific-Kula spreading at chron 34 time (84.00 Ma) was followed by a steady increase in spreading rate, also noted by Mammerickx and Sharman (1988), which culminated between chrons 33y and 30/31. The rate then decreased until chron 28, at which time the angular rate increased sharply until chron

Table 6. Pacific-Farallon Stage Poles

Chron		Latitude	Longitude	Finite Angle	Whole-Rates (deg/my)		
From	To	°N	°E	(deg)	Best	Maximum	Minimum
34	33o	1.0	197.0	2.94	0.768	0.874	0.632
33o	33y	66.0	64.2	4.64	0.791	0.835	0.691
33y	32a	66.0	64.2	1.55	0.556	0.624	0.480
32a	30/31	66.0	64.2	2.22	0.729	0.811	0.645
30/31	29	66.0	64.2	1.87	0.710	0.778	0.640
29	28	66.0	64.2	0.81	0.721	0.875	0.553
28	27	66.0	64.2	1.32	0.931	1.059	0.781
27	26	66.0	64.2	2.11	0.752	0.844	0.658
26	25	66.0	64.2	1.19	0.771	0.861	0.659
25	24	77.4	178.3	4.11	1.245	1.335	1.147

Note: The Pacific plate remains fixed and the rotation of the Farallon plate during the time spanned by a pair of chrons is described going forward in time (right hand rule).

Table 7. Pacific-Farallon End-Member Poles

Chron		Latitude	Longitude	Whole Rate
From	To	°N	°E	(deg/my)
34	33o	-11.0	17.0	0.768
34	33o	9.0	17.0	0.768
34	33o	-1.0	22.0	0.768
34	33o	-1.0	12.0	0.768
33o	33y	59.3	57.4	0.791
33o	33y	71.3	73.5	0.791
33o	33y	67.2	58.1	0.791
33o	33y	64.8	69.3	0.791
33y	32a	59.3	57.4	0.556
33y	32a	71.3	73.5	0.556
33y	32a	67.2	58.1	0.556
33y	32a	64.8	69.3	0.556
32a	30/31	59.3	57.4	0.729
32a	30/31	71.3	73.5	0.729
32a	30/31	67.2	58.1	0.729
32a	30/31	64.8	69.3	0.729
30/31	29	59.3	57.4	0.710
30/31	29	71.3	73.5	0.710
30/31	29	67.2	58.1	0.710
30/31	29	64.8	69.3	0.710
29	28	59.3	57.4	0.721
29	28	71.3	73.5	0.721
29	28	67.2	58.1	0.721
29	28	64.8	69.3	0.721
28	27	59.3	57.4	0.931
28	27	71.3	73.5	0.931
28	27	67.2	58.1	0.931
28	27	64.8	69.3	0.931
27	26	59.3	57.4	0.752
27	26	71.3	73.5	0.752
27	26	67.2	58.1	0.752
27	26	64.8	69.3	0.752
26	25	59.3	57.4	0.771
26	25	71.3	73.5	0.771
26	25	67.2	58.1	0.771
26	25	64.8	69.3	0.771
25	24	80.5	142.1	1.245
25	24	72.1	195.6	1.245
25	24	80.7	200.0	1.245
25	24	72.9	166.1	1.245

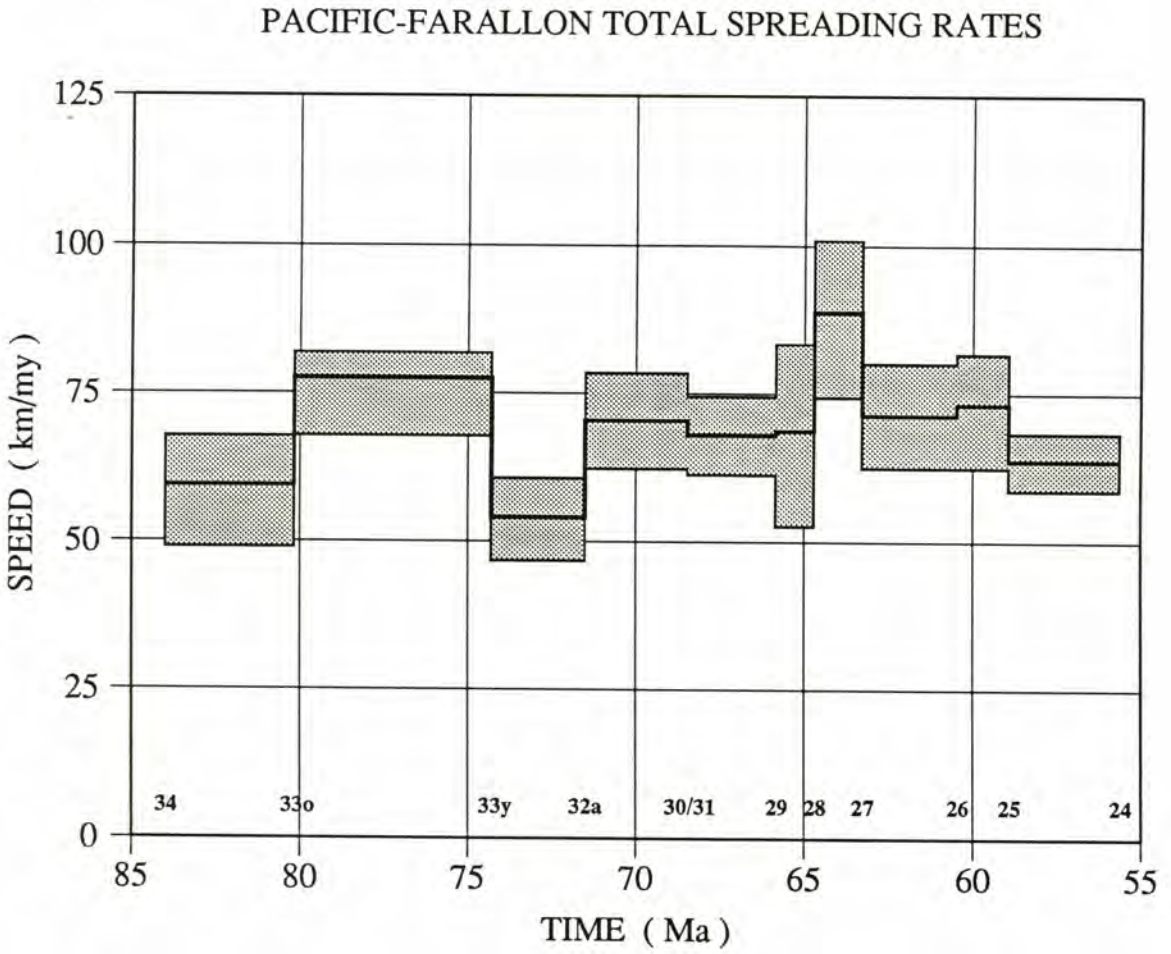

Figure 9. Pacific-Farallon linear velocities determined at the apexes of the GMB. Central black line represents the best-fit linear velocity for each of the time periods shown. Shaded regions show the 1 σ uncertainties for the best-fit linear velocities.

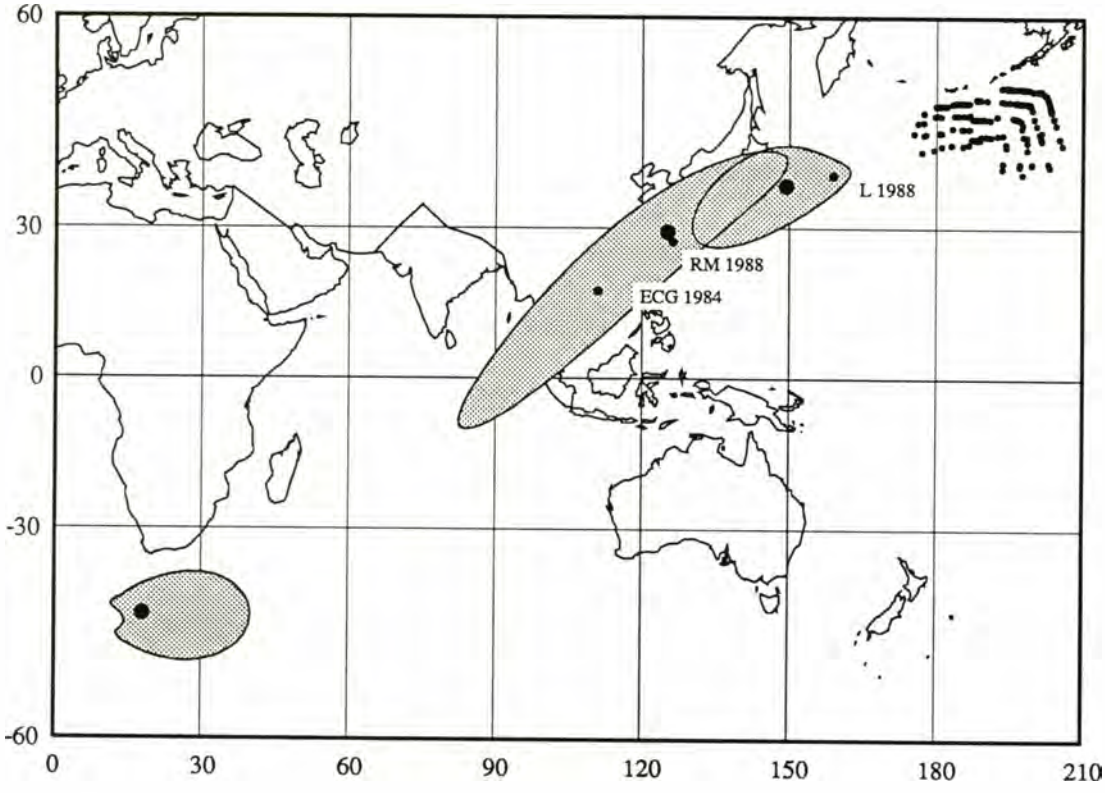

Figure 10. Updated Pacific-Kula relative motion poles from Figure 7 (large black dots) compared with those from previous workers. Smaller dots represent stage poles of Engebretson, Cox, and Gordon (1984) (ECG) ; Rosa and Molnar (1988) (RM); and Lonsdale (1988) (L). Both the ECG and RM stage poles reconstruct chron 32 onto chron 25. Lonsdale's stage pole reconstructs chron 23 onto chron 21 (chrons of the Kula remnant, shown on Figure 1).

27. The angular half-rate decreased rapidly from chron 27 to chron 26, then increased from chron 26 through chron 24.

This history of rapidly changing spreading rates is different from previous interpretations. Early workers estimated Pacific-Kula spreading rates were in the range of 70 - 90 km/my from chron 32 to chron 25 (Hayes and Heirtzler, 1968; Byrne, 1979; Rosa and Molnar, 1988). These workers did not attempt a detailed analysis of spreading rates over shorter time intervals. Engebretson et al. (1984) documented a steady decrease in Pacific-Kula spreading rate from chron 32 to chron 25, when spreading again accelerated, but they had no control over pre-chron 32 spreading rates.

Pole migrations and changes in angular rate presented here are necessarily shown as occurring at discrete times. The best-fit pole location for time interval 2 lies between those for time intervals 1 and 3 (Figure 6a) because it may represent a motion averaged over the time spanned by the data. Thus the overlap of confidence regions surrounding pole locations may result from this averaging effect. Changes in spreading rate also may have occurred within the chosen intervals, with more abrupt changes in actual rates subdued by averaging over the time 'window' of the interval.

Velocity Triangle Analysis

Symmetric accretion at a spreading ridge is an important assumption in the kinematic analysis of plate tectonics. However, asymmetric sea-floor spreading has been documented across numerous spreading centers and is thought to be an important tectonic process (Weissel and Hayes, 1971; Hayes, 1976). Asymmetric sea-floor

accretion can have significant effects on the evolution of plate boundaries in both time and space (Hayes, 1976). The assumption of symmetric seafloor accretion was tested across the ridges near the Pacific-Farallon-Kula triple junction by comparing the observed triple junction motion as recorded by the apex of the GMB on the Pacific plate with the motion predicted by the updated Pacific-Kula and Pacific-Farallon relative motions presented here.

Predicted Triple Junction Velocity

The assumption of symmetric seafloor spreading allowed angular half-rates for a given time interval to be doubled, yielding whole spreading rates. Predicted motion of the PFK triple junction in velocity space was derived by constructing Pacific-Farallon-Kula velocity triangles assuming symmetric seafloor spreading with ridge segments orthogonal to transforms. The limbs of a velocity triangle for a given time interval represent the modeled Pacific-Kula and Pacific-Farallon linear velocities determined from the best-fit Pacific-Kula and Pacific-Farallon stage poles for that time interval. As illustrated in Figure 11a, the intersection of the perpendicular bisectors of these vectors predicts the instantaneous linear velocity of the PFK triple junction for the given time interval.

Confidence regions around predicted PFK triple junction velocities were derived as follows. For each time interval there are 7 Pacific-Kula and 7 Pacific-Farallon relative motion poles. These seven poles include the best-fit pole location and spreading rate, the best-fit pole location with the maximum uncertainty in spreading rate, the best-fit pole location with the minimum uncertainty in rate, and four end-member

Figure 11. (a) Hypothetical example of a velocity triangle showing Pacific-Kula and Pacific-Farallon linear velocities determined at the apexes of the GMB from updated relative motions. Solid dot shows the "predicted" triple junction migration vector, which is located at the intersection of the perpendicular bisectors of the model linear velocities. Square represents an "observed" triple junction velocity. Note that in this schematic example, the "observed" triple junction velocity might indicate asymmetric spreading across the Pacific-Kula and Pacific-Farallon ridges, with the Pacific plate receiving more plate in each case.

(b) Uncertainties around the predicted triple junction migration are controlled by the perpendicular bisectors of the 49 possible combinations which result from the 7 Pacific-Kula and 7 Pacific-Farallon linear velocities for the given time interval.

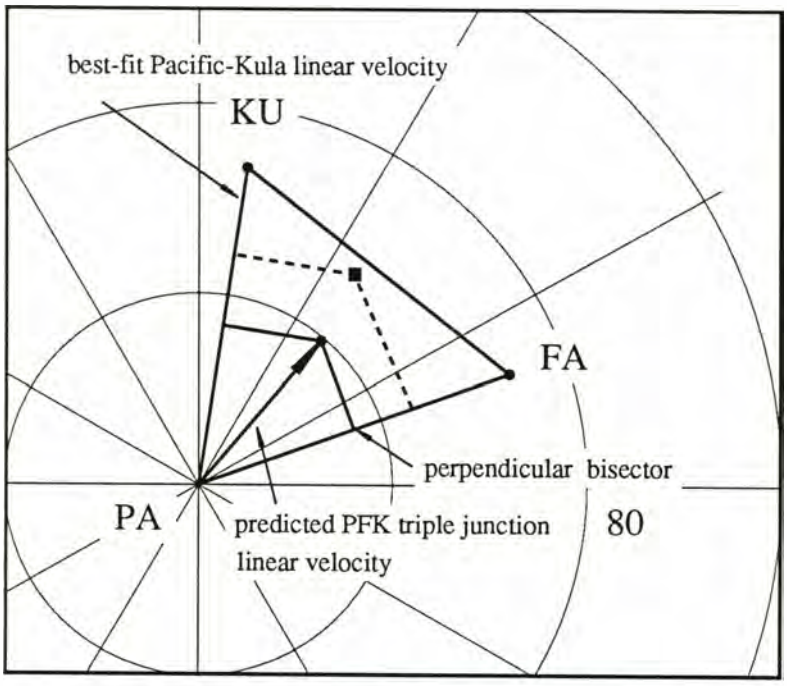
best-fit Pacific-Kula linear velocity
KU
FA
perpendicular bisector
PA
predicted PFK triple junction
linear velocity
80

(a)

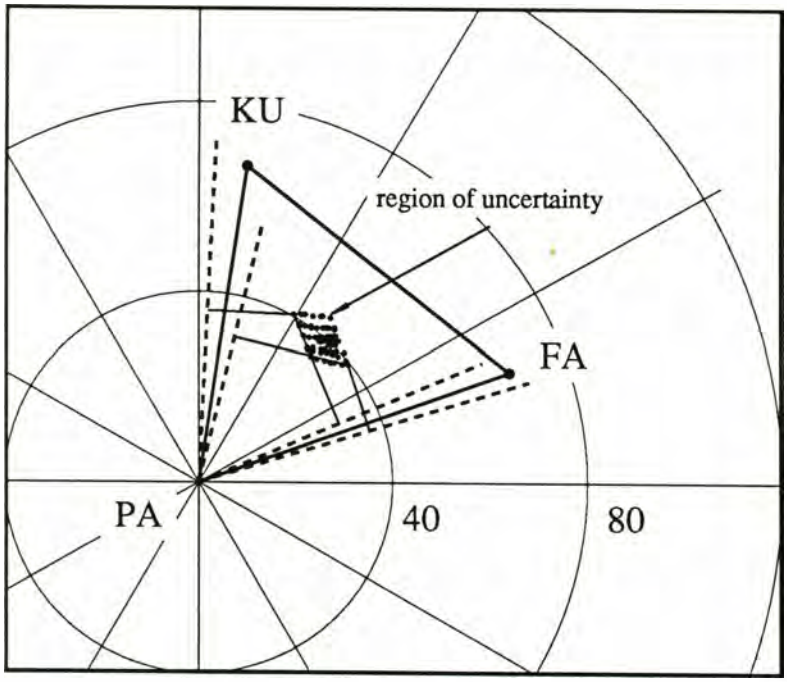
KU
region of uncertainty
FA
PA
40
80

(b)

poles with their associated spreading rates (Tables 3, 4, 6, and 7). The Pacific-Kula and Pacific-Farallon instantaneous poles were converted into linear velocities at the intersection of the Pacific-Kula and Pacific-Farallon isochrons (at the apex of the GMB) that define the older end of the given time interval. The combination of the 7 Pacific-Kula and 7 Pacific-Farallon linear velocities results in 49 perpendicular bisector intersections. One intersection, from the two best-fit instantaneous poles, is the predicted PFK triple-junction velocity. The remaining 48 combinations define the uncertainty region around this predicted triple-junction velocity (Figure 11b).

Observed Triple Junction Velocity

Linear velocities describing the observed migration of the PFK triple junction were obtained along the digitized points of the PFK triple-junction trajectory (see Figure 1). Data for the location of the GMB at chron 34 were supplemented with data from Mammerickx and Sharman (1988). These points were used to determine instantaneous linear velocity vectors for the given time intervals relative to a fixed Pacific plate (Table 8). The azimuth represents the direction (in degrees east of north) of a great circle drawn between two successive points along the GMB while the speed is the linear distance between the successive points divided by the time spanned.

The method presented here for testing the assumption of symmetric spreading across the Pacific-Kula and Pacific-Farallon ridges during the time intervals studied assumes that the observed linear velocity of the triple junction should fall within the uncertainty region of the predicted triple junction linear velocity. Symmetric spreading across both ridges would be consistent with a velocity triangle similar to that in

Table 8. Linear velocities of the PFK triple junction relative to a fixed Pacific plate

Chron		Latitude	Longitude	Azimuth	Speed
From	To	°N	°E	°E	km/my
34	33o	44.9	191.5	70.6	45.38
33o	33y	45.4	193.6	49.1	41.19
33y	32a	46.8	196.0	25.1	44.11
32a	30/31	47.8	196.7	36.9	59.88
30/31	29	49.1	198.2	42.5	40.39
29	28	49.8	199.2	52.0	32.11
28	27	50.0	199.6	41.6	52.56
27	26	50.5	200.3	69.5	34.71
26	25	50.8	201.6	31.9	51.17
25	24	51.4	202.2	3.6	64.16

Figure 11b. In Figure 11b, the observed triple junction linear velocity falls within the predicted linear velocity region, indicating the assumption of symmetric spreading across both ridges for this time interval cannot be rejected.

Results

Based on the test outlined above, the hypothesis of symmetric spreading cannot be rejected for time intervals 2, 3, 5-8, and 10 because the observed triple-junction linear velocity falls within the uncertainty region for the predicted triple-junction linear velocity (Figure 12). Below the other time intervals are examined to assess whether discrepancies resulted from peculiarities in the data or from asymmetric spreading.

Results for time interval 1 produce a large uncertainty region for the predicted triple-junction velocity because of the large uncertainties in Pacific-Farallon end-member poles. The observed linear velocity of the triple junction during this time interval is also poorly constrained because of the the large uncertainty in the location of the triple junction for chron 34 and 33o (Figure 13). Therefore, the poor agreement between the observed and predicted triple junction linear velocity for this time interval can not be resolved.

Results for time interval 4 show the observed triple-junction velocity lying well outside of the predicted uncertainty region but within the velocity triangle. This discrepancy may result from the unique curvature of chron 31 as seen on the tectonic chart of Atwater and Severinghaus (1989) (Figure 13). The Pacific-Kula chron 31 appears to bulge northward near its intersection with the Pacific-Farallon chron 31.

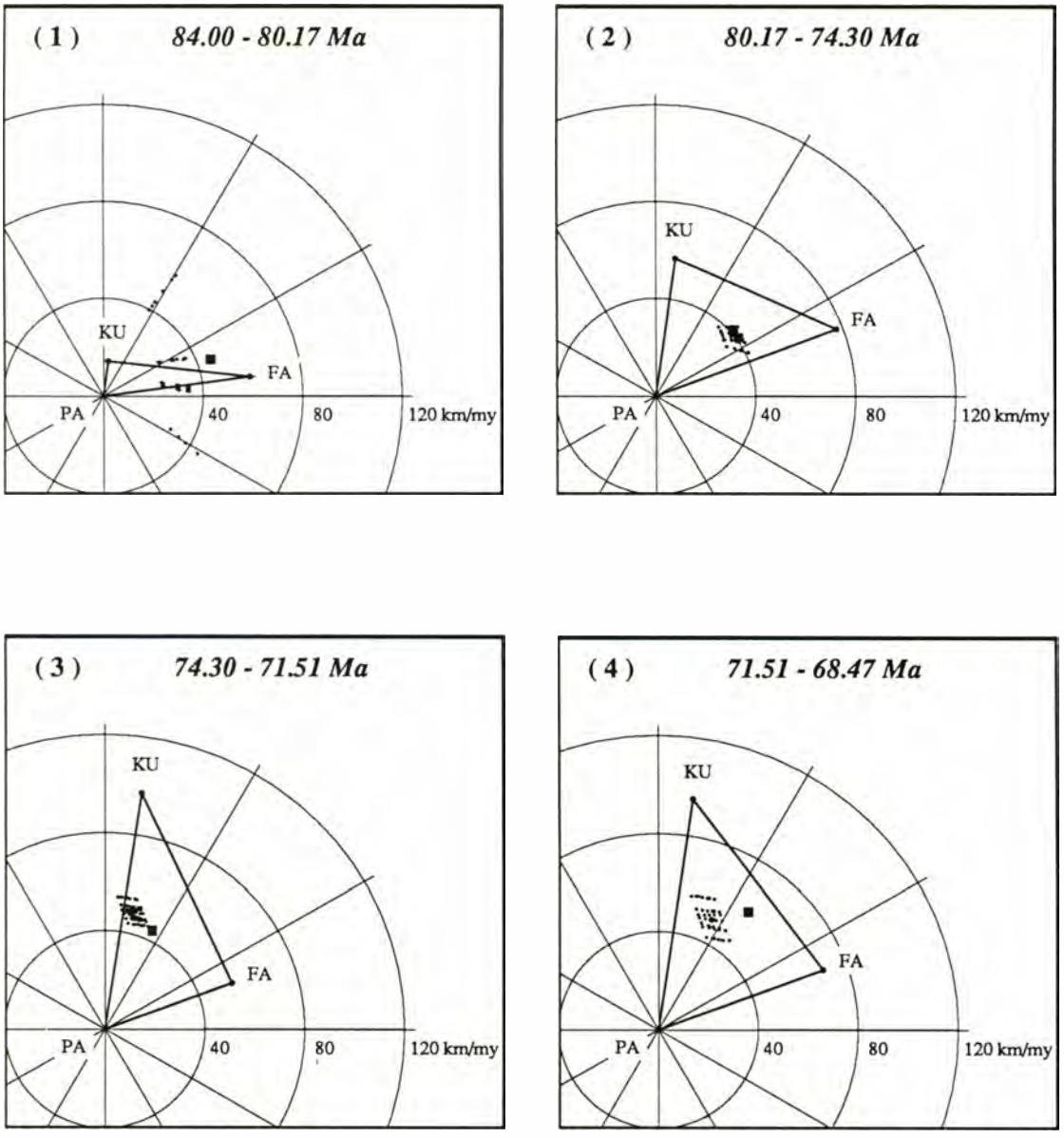

Figure 12. Velocity triangles for time intervals 1 through 10 showing observed (solid squares) and predicted (solid dots) linear velocities for migration of the PFK triple junction, and associated uncertainties. Time interval and ages are shown at the top of each velocity triangle. See text for discussion of intervals 4 and 9.

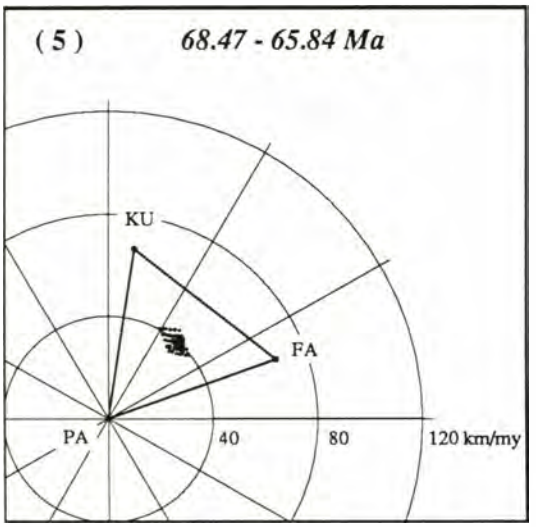
(5)
68.47 - 65.84 Ma
KU
FA
PA
40
80
120 km/my

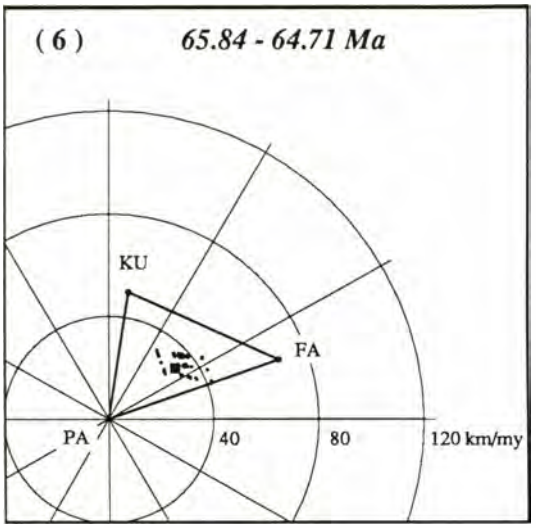
(6)
65.84 - 64.71 Ma
KU
FA
PA
40
80
120 km/my

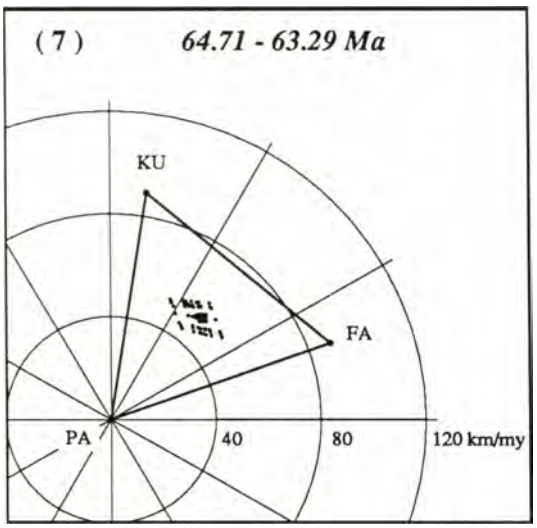
(7)
64.71 - 63.29 Ma
KU
FA
PA
40
80
120 km/my

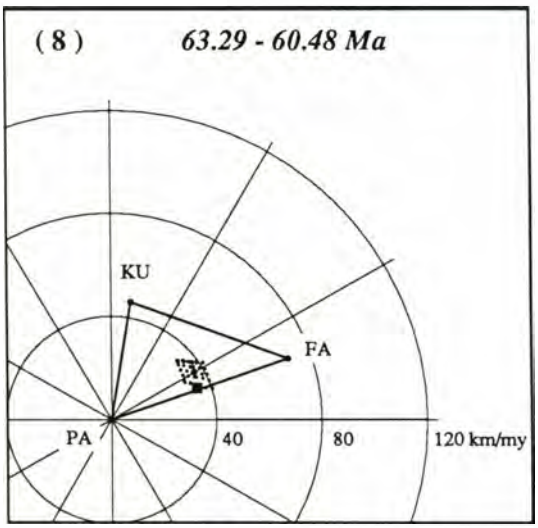
(8)
63.29 - 60.48 Ma
KU
FA
PA
40
80
120 km/my

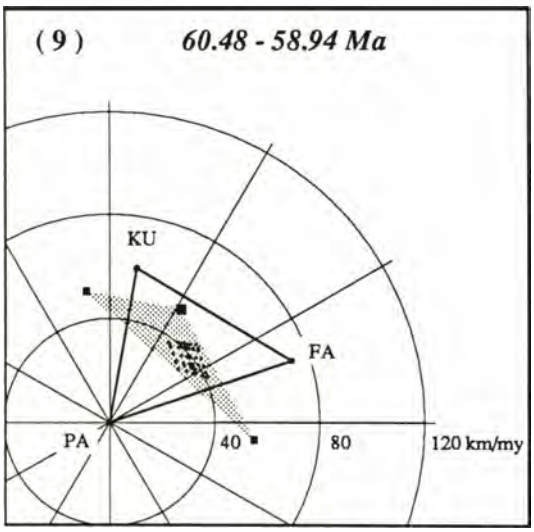
(9)
60.48 - 58.94 Ma
KU
FA
PA
40
80
120 km/my

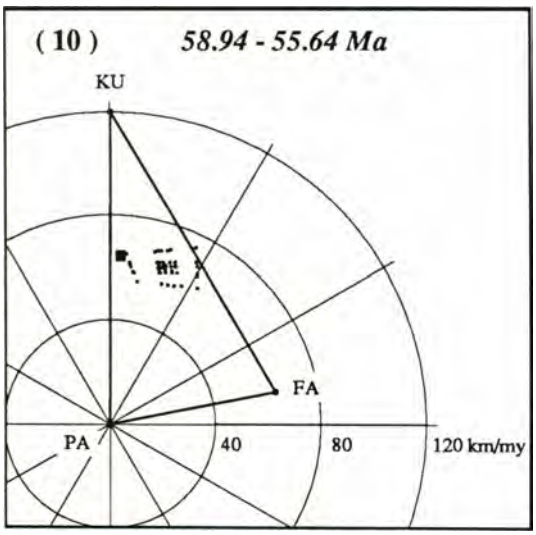
(10)
58.94 - 55.64 Ma
KU
FA
PA
40
80
120 km/my

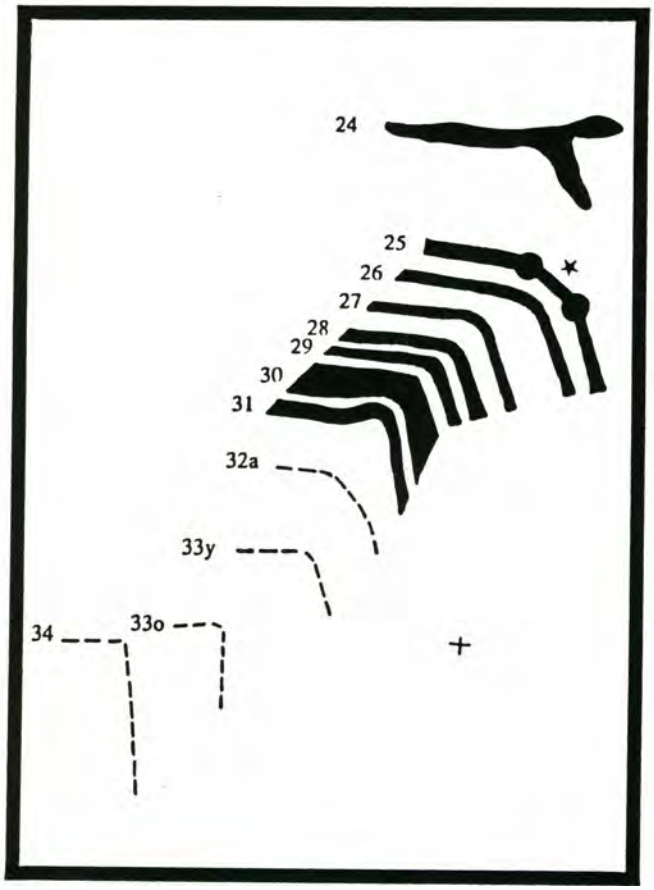

Figure 13. Schematic magnetic isochron map of the GMB after Atwater and Severinghaus (1989). Poorly constrained chron boundaries which are based on a small number of data points are represented by dashed lines. Note the northward bulge of chron 31 at the GMB, which may suggest some type of triple junction reorganization at this time. Also note the poorly defined bight location of chron 25 which could lie at any of three locations. The location used in this study is the central point in the gradual bend of chron 25 represented here by the star. The triple junction could also have lain at either end of the bend, at locations represented here by solid dots. The tic mark represents 200° E, 45° N.

This northward bulging chron pattern is unique to this time interval and suggests that some type of triple junction reorganization occurred at this time. The observed triple junction velocity is faster than the predicted velocity, implying that the Pacific plate received more plate than the Kula or Farallon plates. Since the Pacific-Kula component of the observed triple-junction velocity lies within the corresponding uncertainty region, the assumption of symmetric spreading is indicated for that ridge. However, there may have been asymmetric spreading across the Pacific-Farallon ridge, with the Pacific side receiving more plate than the Farallon side.

The result for time interval 9 shows poor agreement between the observed and predicted triple-junction migrations. The uncertainty region is centrally located in the velocity triangle indicating similar Pacific-Kula and Pacific-Farallon spreading parameters. Engebretson et al. (1984) proposed that at chron 25 the Pacific-Kula ridge abruptly accelerated and the Pacific-Farallon spreading direction changed. Reorganization at chron 25 is a probable cause for the large discrepancy between the observed and predicted triple junction velocities. The discrepancy might be due to error in picking the observed triple junction from the poorly defined intersection of the Pacific-Kula chron 25 and the Pacific-Farallon chron 25 (Figure 13). A central point in the gradual bend of chron 25 was chosen as the best estimate for the triple junction location. However, the triple junction location could have lain in other locations for this time interval. Linear velocities for the observed triple junction were also determined at each end of the chron 25 bend (Figure 13) and used to constrain an uncertainty region for the observed triple junction velocity. This observed uncertainty region entirely encompasses the predicted uncertainty region. Thus the uncertainty in

the observed velocity for this time interval is such that the assumption of symmetric spreading cannot be rejected.

Interpretation

Isochrons of the Great Magnetic Bight provide a unique data set through which the assumption of symmetric spreading has been tested. Results of the analysis indicate that the assumption of symmetric spreading is valid for most of the time intervals. Exceptions are time intervals 4 and 9 when asymmetric and/or oblique spreading may explain the discrepancies between predicted and observed triple-junction velocities. The remaining time intervals show that the PFK triple-junction velocity, as observed on the present-day Pacific plate, behaves as would be expected under the assumed conditions of symmetric seafloor accretion. An important result of the velocity-triangle analysis is that the PFK triple-junction migration agrees well with the new Pacific-Kula and Pacific-Farallon relative-motion poles. This fact highlights the high degree of consistency between the two types of data analyzed (one being the fracture zone and magnetic chron data and the second being the observed velocity of the PFK triple junction).

Conclusions

New relative motion poles describing Pacific-Kula motion have provided new constraints on spreading rate and pole location changes across the Pacific-Kula ridge. By analyzing Pacific-Kula motions over the shortest possible time intervals, numerous changes in pole location and spreading half-rates were found. This type of detailed

tectonic analysis might prove useful in deciphering complex plate boundary changes.

In future work, uncertainties in poles of relative motion determined by a similar method might be minimized by further reducing uncertainties assigned to the input data. What is required to reduce the assigned uncertainties is that fracture zone azimuths be better known, from more detailed bathymetry or more closely spaced ship tracks, and that chron ages be better known from more precise magnetostratigraphy (preferably independent of the assumption of constant or symmetric seafloor spreading elsewhere). The better constrained confidence regions resulting from smaller assigned uncertainties might show additional variations in stage pole locations. Future work might also include a thorough analysis of the systematic errors in chron location picks which result from anomalous skewness seen in the observed Pacific-Kula anomaly profiles. Petronotis and Gordon (1989) found that skewness differs significantly between adjacent chrons. Values of skewness could be assigned to each Pacific-Kula anomaly based on anomalous skewness. Spreading rates determined between adjacent chrons could then be better approximated by taking into account the systematic errors induced by skewness, resulting in a more precise Pacific-Kula spreading history.

The results of this work have important implications for North America relative motions and tectonics. Results presented here show that spreading rates were slower from 84.00 to 74.30 Ma than was previously assumed (Engebretson et al., 1984). These slower initial Pacific-Kula spreading rates and other rate changes found allow for a more detailed understanding of Kula-Farallon boundary evolution. Variations that are not synchronized between the Pacific-Kula (Figure 8) and Pacific-Farallon (Figure 9) ridges should result in variable Kula-Farallon spreading velocities.

Interaction of variable Kula-Farallon spreading velocities with North America predict much more complicated interaction of the ridge and adjacent plates with North America than accounted for in Wells et al., (1984) and Engebretson et al., (1985). Variable Kula-Farallon spreading velocities might facilitate rifting of North America, coastwise transport of rifted and allocthonous blocks, and terrane amalgamation. It is clear that as analyses of oceanic-oceanic plate interactions become better defined, our ability to decipher relationships between the geologic record and oceanic-continental plate interactions will improve.

REFERENCES

Atwater, T., and H. W. Menard, Magnetic lineations in the northeast Pacific, Earth Planet. Sci. Lett. , 7 , 445-450, 1970.

Atwater, T., and J. Severinghaus, Tectonic maps of the northeast Pacific, in: *The Geology of North America: The Eastern Pacific Ocean and Hawaii, DNAG Ser.*, vol. N, edited by E. L. Winterer, D. M. Hussong, and R. W. Decker, Geological Society of America, Boulder, Colo., pp. 15-20, 1989.

Berggren, W. A., D. V. Kent, J. J. Flynn, and J. A. Van Couvering, Cenozoic geochronology, Geol. Soc. Amer. Bull. , 96 , 1407-1418, 1985.

Bevington, P. R., Data reduction and error analysis for the physical sciences, McGraw-Hill, New York, 336pp., 1969.

Byrne, T., Late Paleocene demise of the Kula-Pacific spreading center, Geology , 7 , 341-344, 1979.

Chase, T. E., H. W. Menard, and J. Mammerickx, Bathymetry of the North Pacific, Tech. Rep. Ser. TR 28 - 29 , 2 , 3 Inst. of Mar. Resour., Scripps Inst. of Oceanogr., Univ. of Calif., San Diego, La Jolla, 1970a.

Chase, C. G., The N-plate problem of plate tectonics, Geophys. J. R. Astr. Soc. , 29 , 117, 1972.

DeLong, S. E., P. J. Fox, and F. W. McDowell, Subduction of the Kula ridge at the Aleutian Trench, Geol. Soc. Amer. Bull. , 89 , 83-95, 1978.

DeMets, C., R. G. Gordon, D. F. Argus, and S. Stein, Current plate motions, Geophys. J. Int. , 101 , 425-478, 1990.

Elvers, D. J., G. Peter, and R. L. Moses, Analysis of magnetic lineations in the North Pacific (abstract), Trans. Am. Geophys. Union , 48 , 89, 1967a.

Elvers, D. J., C. C. Mathewson, R. E. Kohler, and R. L. Moses, Systematic ocean surveys by the USC and GSS Pioneer 1961-1963, Coast and Geodetic Survey Opera- tional Data Report C and GSDR-1 , 19pp., U.S. Coast and Geod. Surv., Washington, D.C., 1967b.

Engebretson, D. C., A. Cox, and R. Gordon, Relative motions between oceanic plates of the Pacific basin, J. Geophys. Res. , 89 , 10,291-10,310, 1984.

Engebretson, D. C., A. Cox, and R. Gordon, Relative motions between oceanic and continental plates *in* the Pacific basin, Spec. Pap. Geol. Soc. Amer. , 206 , 59 pp., 1985.

Erickson, B. H., and P.J. Grim, Profiles of magnetic anomalies south of the Aleutian island arc, Geol. Soc. Amer. Bull. , 80 , 1387-1390, 1969.

Erickson, B. H., D. K. Rea, and F. P. Naugler, Chinook trough: A probable consequence of north-south sea-floor spreading, (abstract) EOS , 50 , 633, 1969.

Grim, P. J., and B. H. Erickson, Fracture zones and magnetic anomalies south of the Aleutian trench, J. Geophys. Res. , 74 , 1488-1494, 1969.

Grow, J. A., and T. Atwater, Mid Tertiary tectonic transition in the Aleutian island arc, Geol. Soc. Amer. Bull. , 81 , 3715-3722, 1970.

Harland, W. B., Cox, A. V., Llewellyn, P. G., Pickton, C. A. G., Smith, A. G., and R. Walters, A Geologic Timescale, Cambridge University Press, Cambridge, 131pp., 1982.

Hayes, D. E., Nature and implications of asymmetric sea-floor spreading - "Different rates for different plates", Geol. Soc. Amer. Bull. , 87 , 994-1002, 1976.

Hayes, D. E., and J. R. Heirtzler, Magnetic anomalies and their relation to the Aleutian island arc, J. Geophys. Res. , 73 , 4637-4646, 1968.

Kent, D. V., and F. M. Gradstein, A Jurassic to recent chronology, Geol. Soc. Amer. Bull. , 96 , 1419-1427, 1985.

Larson, R., and W. C. Pitman, III, World-wide correlation of Mesozoic magnetic anomalies and its implications, Geol. Soc. Amer. Bull. , 83 , 3645-3662, 1972.

Lonsdale, P., Paleogene history of the Kula plate: Offshore evidence and onshore implications, Geol. Soc. Amer. Bull. , 100 , 733-754, 1988.

Mammerickx, J., and G. F. Sharman, Tectonic evolution of the north Pacific during the Cretaceous quiet period, J. Geophys. Res. , 93 , 3009-3024, 1988.

Mammerickx, J., Large-scale undersea features of the northeast Pacific, in: *The Geology of North America: The Eastern Pacific Ocean and Hawaii, DNAG Ser.*, vol. N, edited by E. L. Winterer, D. M. Hussong, and R. W. Decker, Geological Society of America, Boulder, Colo., pp. 5-13, 1989.

Minster, J. B., T. H. Jordan, P. Molnar, and E. Haines, Numerical modeling of instantaneous plate tectonics, Geophys. J. R. Astr. Soc. , 36 , 541-576, 1974.

Molnar, P., and J. Stock, A method for bounding uncertainties in combined plate reconstructions, J. Geophys. Res. , 90 , 12,537-12,544, 1985.

Peter, G., Magnetic anomalies and fracture pattern in the northeast Pacific Ocean, J. Geophys. Res. , 71 , 5365-5374, 1966.

Petronotis, K. E., and R. G. Gordon, Age dependence of skewness of magnetic anomalies above seafloor formed at the Pacific-Kula spreading center, Geophys. Res. Lett. , 16 , 315-318, 1989.

Pitman, W. C., and D. E. Hayes, Sea-floor spreading in the Gulf of Alaska, J. Geophys. Res. , 73 , 6571-6580, 1968.

Press, W. H., B. P. Flannery, S. A. Teukolsky, and W. T. Vetterling, Numerical Recipes; The art of scientific computing, Cambridge University Press, Cambridge, 818pp., 1986.

Rea, D. K. and J. M. Dixon, Late Cretaceous and Paleogene tectonic evolution of the North Pacific Ocean, Earth Plan. Sci. Lett. , 65 , 145-166, 1983.

Rosa, J. W. C., and P. Molnar, Uncertainties in reconstructions of the Pacific, Farallon, Vancouver, and Kula plates and constraints on the rigidity of the Pacific and Farallon (and Vancouver) plates between 72 and 35 Ma, J. Geophys. Res. , 93 , 2997-3008, 1988.

Shive, P. N., Suggestions for the use of SI units in magnetism, Trans. AM. Geophys Union (EOS) , 67 , 25, 1986.

Weissel, J. K., and D. E. Hayes, Asymmetric seafloor spreading south of Australia, Nature , 231 , 518-522, 1971.

Wells, R. E., D. C. Engebretson, P. D. Snavely, Jr., and R. S. Coe, Cenozoic plate motions and the volcano-tectonic evolution of western Oregon and Washington, Tectonics , 3 , 275-294, 1984.

Woods, M. T., and G. F. Davies, Late Cretaceous genesis of the Kula plate, Earth Planet. Sci. Lett. , 58 , 161-166, 1982.

APPENDIX 1. Pacific-Kula ship track segments and anomaly picks used in this analysis. Ship track identification codes are from NGDC numbering scheme.

Latitude	Longitude	Age (Ma)
POL7103		
44.955	191.027	84.000
45.156	191.020	80.170
46.562	191.026	74.300
POL7103		
45.317	192.490	80.170
46.589	192.535	74.300
POL7103		
46.923	194.472	74.300
POL7103		
45.455	193.527	80.170
46.695	193.557	74.300
C1407		
53.634	203.385	55.640
54.086	203.236	54.290
C1008		
44.370	177.057	74.300
45.530	177.817	71.510
46.698	178.644	68.470
C1008		
47.365	179.224	68.470
48.110	179.723	65.840
48.308	179.883	64.710
48.726	180.215	63.290
49.528	180.960	60.480
C1010		
47.622	186.823	68.470
48.320	186.800	65.840
48.569	186.759	64.710
49.125	186.561	63.290
49.612	186.423	60.480
49.992	186.288	58.940
51.165	185.952	55.640
C1010		
44.370	187.345	84.000
44.838	187.189	80.170
45.696	186.976	74.300
46.335	186.769	71.510
C1010		
44.480	188.490	84.000
44.852	188.511	80.170

Latitude	Longitude	Age (Ma)
C1010		
44.995	189.956	84.000
45.296	190.024	80.170
46.572	189.808	74.300
47.758	189.402	71.510
C1010		
49.650	188.884	68.470
50.424	188.611	65.840
50.662	188.533	64.710
C1109		
43.320	186.289	84.000
44.357	185.864	80.170
45.397	185.506	74.300
46.368	185.150	71.510
47.550	184.727	68.470
48.239	184.463	65.840
48.496	184.359	64.710
49.068	184.113	63.290
C1109		
50.032	196.464	65.840
50.290	196.180	64.710
50.890	195.533	63.290
51.498	194.836	60.480
51.923	194.329	58.940
52.870	193.146	55.640
V2006		
42.923	181.214	84.000
43.743	181.080	80.170
44.809	180.891	74.300
45.798	180.692	
47.571	180.268	68.470
48.200	180.146	65.840
48.343	180.118	64.710
48.699	180.049	63.290
49.170	180.023	60.480
49.460	180.011	58.940
V2111		
51.922	195.349	58.940
C1207		
49.515	180.973	58.940
C1207		
49.532	181.684	58.940

Latitude	Longitude	Age (Ma)
V2112		
46.747	195.984	74.300
47.939	195.656	71.510
49.255	195.271	68.470
50.104	194.994	65.840
50.340	194.934	64.710
50.830	194.809	63.290
51.416	194.658	60.480
51.846	194.546	58.940
53.230	194.195	55.640
SI343505		
49.225	197.493	68.470
49.950	197.512	65.840
50.198	197.527	64.710
50.777	197.218	63.290
51.422	196.872	60.480
51.867	196.647	58.940
SI343505		
51.133	200.122	60.480
51.728	198.932	58.940
53.677	196.147	55.640
SI343505		
49.898	198.552	65.840
50.175	198.355	64.710
50.740	197.892	63.290
51.398	197.248	60.480
51.848	196.950	58.940
SI932005		
43.743	183.507	80.170
45.268	183.542	74.300
SI932005		
43.297	179.518	80.170
SI932005		
45.665	175.488	71.510
46.525	175.883	68.470
47.130	176.290	65.840
47.367	176.547	64.710
47.895	177.282	63.290
48.162	177.723	60.480
YAQ702		
53.410	199.803	55.640

Latitude	Longitude	Age (Ma)
C1208		
48.195	192.316	71.510
49.595	190.895	68.470
50.381	190.247	65.840
50.648	189.945	64.710
C1208		
49.349	195.119	68.470
50.024	196.570	65.840
50.227	197.068	64.710
50.735	198.329	63.290
51.230	199.216	60.480
51.538	199.602	58.940
53.403	201.608	55.640
POL6971		
42.227	177.010	84.000
42.888	177.003	80.170
44.396	177.241	74.300
45.415	177.423	71.510
46.515	177.514	68.470
47.239	177.476	65.840
47.469	177.456	64.710
47.915	177.463	63.290
48.202	177.463	60.480
48.532	177.484	58.940
POL6971		
45.466	179.510	71.510
POL6971		
47.721	189.735	71.510
49.632	189.887	68.470
POL6829		
43.306	185.498	84.000
43.846	185.490	80.170
45.400	185.517	74.300
46.343	185.503	71.510
47.548	185.521	68.470
48.281	185.509	65.840
48.531	185.504	64.710
49.093	185.461	63.290

Latitude	Longitude	Age (Ma)
POL6829		
43.449	186.488	84.000
44.044	186.500	80.170
45.468	186.496	74.300
46.324	186.503	71.510
47.538	186.517	68.470
48.299	186.499	65.840
48.545	186.510	64.710
POL6829		
44.981	190.012	84.000
45.292	190.002	80.170
46.568	190.008	74.300
47.717	189.995	71.510
POL6829		
44.964	190.990	84.000
45.137	191.004	80.170
46.565	190.992	74.300
47.663	190.992	71.510
49.542	192.419	68.470
50.233	193.325	65.840
50.464	193.614	64.710
POL6829		
49.428	193.991	68.470
50.188	194.022	65.840
50.447	194.023	64.710
POL6829		
45.771	181.044	71.510
47.554	180.967	68.470
48.127	180.999	65.840
48.293	181.010	64.710
48.767	181.005	63.290
49.228	180.990	60.480
49.511	180.995	58.940
50.894	180.996	55.640
POL6829		
42.744	180.025	84.000
43.449	179.988	80.170
C1209		
53.213	202.190	55.640
CMAPPI3S		
53.470	202.334	55.640

Latitude	Longitude	Age (Ma)
CMAPPI3S		
53.488	202.412	55.640
CMAPPI3S		
53.488	202.544	55.640
CMAPPI3S		
50.793	201.767	60.480
51.322	201.765	58.940
CMAPPI3S		
50.955	201.420	60.480
51.509	201.419	58.940
53.417	201.394	55.640
CMAPPI3S		
51.817	198.865	58.940
53.488	198.708	55.640
CMAPPI3S		
49.840	199.008	64.710
50.119	198.997	63.290
51.283	198.904	60.480
CMAPPI3S		
51.107	200.629	60.480
51.577	200.559	58.940
53.389	200.439	55.640
CMAPPI3S		
49.897	198.829	65.840
50.137	198.831	64.710
50.711	198.859	63.290
51.293	198.846	60.480
CMAPPI3S		
49.901	198.599	65.840
50.147	198.617	64.710
50.695	198.692	63.290
51.295	198.680	60.480
CMAPPI3S		
49.909	198.356	65.840
50.181	198.378	64.710
50.714	198.412	63.290
51.320	198.452	60.480
51.762	198.483	58.940

Latitude	Longitude	Age (Ma)
CMAPPI3S		
49.057	197.767	68.470
49.923	197.850	65.840
50.225	197.877	64.710
50.764	197.897	63.290
51.360	197.938	60.480
51.810	197.943	58.940
53.507	198.065	55.640
CMAPPI3S		
49.233	197.553	68.470
49.943	197.586	65.840
50.203	197.595	64.710
50.774	197.609	63.290
51.388	197.655	60.480
51.765	197.673	58.940
53.537	197.785	55.640
CMAPPI3S		
49.193	197.288	68.470
49.965	197.342	65.840
50.190	197.361	64.710
50.767	197.367	63.290
51.405	197.392	60.480
51.808	197.412	58.940
CMAPPI3S		
49.231	197.046	68.470
49.956	197.057	65.840
50.224	197.080	64.710
50.789	197.120	63.290
51.385	197.138	60.480
51.813	197.183	58.940
CMAPPI3S		
49.249	196.278	68.470
50.032	196.306	65.840
50.275	196.303	64.710
50.830	196.300	63.290
51.453	196.322	60.480
51.889	196.341	58.940
53.749	196.384	55.640

Latitude	Longitude	Age (Ma)
CMAPPI3S		
49.993	196.822	65.840
50.258	196.831	64.710
50.808	196.827	63.290
51.433	196.850	60.480
51.838	196.868	58.940
53.570	196.946	55.640
CMAPPI3S		
49.146	195.998	68.470
50.043	196.062	65.840
50.316	196.087	64.710
50.853	196.070	63.290
51.476	196.056	60.480
51.877	196.072	58.940
53.628	196.103	55.640
CMAPSU3S		
51.881	195.812	58.940
CMAPSU3S		
51.464	195.532	60.480
51.887	195.524	58.940
CMAPSU3S		
51.468	195.253	60.480
51.889	195.267	58.940
CMAPSU3S		
51.480	195.007	60.480
51.898	194.980	58.940
53.376	194.990	55.640
CMAPSU3S		
51.907	194.748	58.940
CMAPSU3S		
51.489	194.465	60.480
51.909	194.449	58.940
CMAPSU3S		
51.505	194.200	60.480
51.917	194.198	58.940
CMAPSU3S		
48.765	199.165	68.470
49.819	199.108	65.840
50.103	199.073	64.710
50.679	198.949	63.290
51.272	198.912	60.480
51.758	198.856	58.940

Latitude	Longitude	Age (Ma)
CMAPSU3S		
50.687	198.887	63.290
51.282	198.877	60.480
51.782	198.792	58.940
C1210		
53.609	203.231	55.640
54.521	204.227	54.290
C1210		
51.004	201.082	60.480
51.479	201.513	58.940
CMAPPI4S		
51.648	191.965	60.480
51.970	193.303	58.940
CMAPPI4S		
48.455	183.447	64.710
49.061	183.479	63.290
49.545	183.527	60.480
49.877	183.563	58.940
CMAPPI4S		
49.090	184.413	63.290
49.586	184.820	60.480
49.966	185.138	58.940
CMAPPI4S		
48.285	183.663	65.840
48.489	183.664	64.710
49.056	183.722	63.290
49.538	183.723	60.480
C1219		
46.505	177.236	68.470
47.272	178.123	65.840
47.496	178.372	64.710
C1219		
47.977	178.936	65.840
48.117	179.101	64.710
C1220		
44.959	190.932	84.000
45.195	190.727	80.170
46.574	189.448	74.300
47.761	188.155	71.510
CMAPSU4S		
49.594	187.419	68.470

Latitude	Longitude	Age (Ma)
CMAPSU4S		
49.620	187.714	68.470
CMAPSU4S		
49.629	188.207	68.470
50.491	188.172	65.840
50.668	188.165	64.710
CMAPSU4S		
50.479	188.994	65.840
50.728	188.969	64.710
CMAPSU4S		
50.988	193.408	63.290
51.546	193.398	60.480
51.939	193.396	58.940
CMAPSU4S		
50.374	191.031	64.710
51.009	191.030	63.290
CMAPSU4S		
49.632	186.679	60.480
49.993	186.666	58.940
51.218	186.584	55.640
CMAPSU4S		
49.116	185.950	63.290
49.659	185.897	60.480
49.976	185.876	58.940
51.161	185.800	55.640
CMAPSU4S		
49.126	185.698	63.290
49.658	185.652	60.480
49.955	185.626	58.940
51.192	185.535	55.640
CMAPSU4S		
49.654	185.407	60.480
49.981	185.372	58.940
51.141	185.279	55.640
CMAPSU4S		
49.673	185.125	60.480
49.961	185.109	58.940
51.167	185.007	55.640
CMAPSU4S		
49.592	184.889	60.480
49.938	184.861	58.940
51.126	184.765	55.640

Latitude	Longitude	Age (Ma)
CMAPSU4S		
49.556	184.375	60.480
49.930	184.364	58.940
CMAPSU4S		
49.525	184.123	60.480
49.924	184.079	58.940
CMAPSU4S		
49.078	183.943	63.290
49.548	183.868	60.480
49.906	183.835	58.940
CMAPSU4S		
49.052	183.266	63.290
49.576	183.300	60.480
49.893	183.300	58.940
CMAPSU4S		
51.291	182.806	55.640
CMAPSU4S		
49.287	182.240	60.480
49.574	182.240	58.940
51.170	182.323	55.640
CMAPSU4S		
49.563	181.995	58.940
51.128	182.049	55.640
CMAPSU4S		
49.553	181.732	58.940
CMAPSU4S		
49.241	181.217	60.480
49.562	181.219	
51.071	181.245	55.640
CMAPSU4S		
49.522	180.711	58.940
50.899	180.726	55.640
CMAPSU4S		
49.517	180.452	58.940
50.833	180.440	55.640
CMAPSU4S		
49.369	180.189	60.480
49.545	180.189	58.940
50.917	180.175	55.640
CMAPSU4S		
49.523	179.989	58.940
50.853	179.948	55.640

Latitude	Longitude	Age (Ma)
CMAPPI5A		
43.295	183.100	84.000
43.903	183.072	80.170
45.076	183.180	74.300
46.432	183.270	71.510
47.538	183.292	68.470
CMAPSU5A		
44.372	187.462	84.000
44.838	187.448	80.170
46.182	187.352	74.300
47.805	187.277	71.510
CMAPSU5A		
47.799	187.520	71.510
CMAPSU5A		
44.414	187.669	84.000
44.838	187.658	80.170
CMAPSU5A		
44.356	187.923	84.000
44.787	187.923	80.170
46.481	187.826	74.300
47.773	187.742	71.510
CMAPSU5A		
44.417	188.150	84.000
44.808	188.138	80.170
46.502	188.070	74.300
47.781	188.035	71.510
CMAPSU5A		
44.458	188.320	84.000
44.788	188.308	80.170
46.523	188.301	74.300
47.746	188.265	71.510
CMAPSU5A		
44.488	188.622	84.000
44.834	188.606	80.170
46.540	188.542	74.300
47.741	188.527	71.510
CMAPSU5A		
44.394	188.836	84.000
44.772	188.826	80.170
46.473	188.817	74.300

Latitude	Longitude	Age (Ma)
CMAPSU5A		
44.547	189.112	84.000
45.264	189.092	80.170
46.539	189.013	74.300
47.752	188.987	71.510
CMAPPI5C		
46.435	196.448	74.300
47.844	196.489	71.510
CMAPPI5C		
46.741	196.218	74.300
47.878	196.228	71.510
CMAPPI5C		
46.811	195.956	74.300
47.886	196.008	71.510
CMAPPI5C		
46.868	195.517	74.300

APPENDIX 2. Pacific-Farallon ship track segments and anomaly picks used in this analysis. Ship track identification codes are from NGDC numbering scheme.

Latitude	Longitude	Age (Ma)
POL7103		
40.177	192.335	84.000
40.296	193.426	80.170
40.522	195.794	74.300
40.691	196.995	71.510
40.795	198.378	68.470
40.958	199.478	65.840
41.005	199.881	64.710
41.111	200.794	63.290
POL7103		
47.052	197.535	71.510
47.469	198.864	68.470
47.858	199.966	65.840
48.099	200.432	64.710
POL7103		
49.566	199.247	65.840
49.422	199.907	64.710
49.079	201.017	63.290
C1407		
53.107	202.136	55.640
C1010		
51.013	201.190	60.480
51.017	202.474	58.940
51.013	204.328	55.640
C1109		
42.846	191.939	84.000
43.649	194.202	80.170
44.840	197.529	74.300
45.190	198.463	71.510
45.588	199.769	68.470
C1109		
52.963	202.278	55.640
SI343505		
46.183	199.508	68.470
45.602	201.013	65.840
SI343505		
51.522	201.093	58.940
52.488	202.798	55.640

Latitude	Longitude	Age (Ma)
SI343505		
48.073	200.612	64.710
48.013	201.657	63.290
47.987	203.132	60.480
47.983	203.917	58.940
48.068	205.600	55.640
YAQ701		
44.986	200.119	68.470
45.022	201.398	65.840
45.044	202.060	64.710
45.031	203.017	63.290
45.014	204.420	60.480
44.982	205.249	58.940
POL6623		
44.999	205.183	58.940
45.358	206.729	55.640
POL7004		
46.372	203.781	60.480
46.904	204.452	58.940
47.333	206.015	55.640
POL7004		
43.871	200.396	68.470
44.661	201.453	65.840
45.060	201.994	64.710
POL7001		
43.822	205.032	60.480
43.943	205.705	58.940
POL6971		
44.374	198.530	71.510
POL6971		
45.254	197.712	71.510
POL6829		
48.997	198.343	68.470
49.007	199.574	65.840
49.012	200.115	64.710
49.013	201.128	63.290
49.007	202.619	60.480
49.001	203.416	58.940
49.021	205.043	55.640

Latitude	Longitude	Age (Ma)
POL6829		
49.334	202.556	60.480
49.070	203.379	58.940
48.472	205.433	55.640
C1209		
53.213	202.190	55.640
C1209		
49.005	202.617	60.480
50.786	202.615	58.940
POL6839		
50.075	202.201	60.480
49.687	203.196	58.940
48.984	205.090	55.640
CMAPPI35		
53.470	202.334	55.640
CMAPPI35		
49.977	202.269	60.480
51.080	202.253	58.940
52.748	202.260	55.640
CMAPPI35		
49.120	202.550	60.480
51.003	202.457	58.940
CMAPPI35		
52.705	202.540	55.640
CMAPPI35		
52.730	202.523	55.640
CMAPPI35		
50.403	202.835	58.940
CMAPPI35		
50.012	203.048	58.940
53.592	203.146	55.640
CMAPPI35		
53.642	203.433	55.640
CMAPPI35		
49.220	203.281	58.940
CMAPPI35		
48.804	203.496	58.940

Latitude	Longitude	Age (Ma)
	CMAPPI35	
53.626	203.698	55.640
	CMAPPI35	
49.414	201.014	63.290
	CMAPSU3S	
49.566	204.833	55.640
	CMAPSU3S	
52.740	202.371	55.640
	CMAPPI5B	
39.330	196.397	74.300
39.316	197.564	71.510
39.267	199.077	68.470
	CMAPSU5B	
40.533	200.105	64.710
40.544	201.016	63.290
40.567	202.402	60.480
40.583	203.128	58.940
	CMAPSU5B	
41.170	192.163	84.000
41.178	193.531	80.170
41.107	196.257	74.300
41.088	197.028	71.510
41.051	198.351	68.470
41.058	199.440	65.840
41.076	200.008	64.710
41.095	200.805	63.290
41.136	202.100	60.480
41.118	202.862	58.940

Latitude	Longitude	Age (Ma)
CMAPPI5C		
45.889	201.466	65.840
46.124	201.664	64.710
46.692	202.218	63.290
47.703	203.258	60.480
47.847	203.984	58.940
CMAPPI5C		
45.145	197.349	74.300
46.420	197.401	71.510
CMAPPI5C		
47.505	197.212	71.510
CMAPPI5C		
45.617	196.887	74.300
47.661	196.949	71.510
CMAPPI5C		
45.982	196.687	74.300
47.797	196.752	71.510
CMAPSU5C		
44.047	202.878	64.710
44.782	203.133	63.290
46.526	203.732	60.480
CMAPSU5C		
46.039	199.584	68.470
46.862	200.457	65.840
47.231	200.812	64.710